inhibit the overall mRNA synthesis (data not shown), suggesting that celecoxib-dependent Ca^{2+}-increase induces PUMA through up-regulation of both ATF4 and CHOP.

We also examined the participation of calpain in celecoxib-induced up-regulation of PUMA using an inhibitor of calpain, Z-Leu-Leu-H. We reported that Z-Leu-Leu-H inhibited the celecoxib-dependent activation of calpain and apoptosis [9]. Addition of Z-Leu-Leu-H did not affect the celecoxib-dependent up-regulation of PUMA (data not shown), suggesting that calpain is not involved in celecoxib-induced up-regulation of PUMA.

Role of up-regulation of PUMA in celecoxib-induced apoptosis

We then used the siRNA technique to examine the contribution of celecoxib-induced up-regulation of PUMA in celecoxib-induced Bax activation and translocation, mitochondrial outer membrane permeabilization (release of cytochrome *c* into the cytosol) and induction of apoptosis. We confirmed that transfection of a siRNA for PUMA inhibited the celecoxib-dependent up-regulation of *PUMA* mRNA (Fig. 4A) and PUMA protein (Fig. 4B). FACS analysis showed that this transfection partially suppressed celecoxib-induced apoptosis (Fig. 4C). We also found that this transfection partially suppressed celecoxib-dependent activation of caspase 3 (data not shown), suggesting that the up-regulation of PUMA is involved in celecoxib-induced apoptosis.

As shown in Fig. 4D, the amount of cytochrome *c* in the cytosol fraction increased in the presence of celecoxib and this increase was partially suppressed by the transfection of siRNA for PUMA, suggesting that celecoxib-dependent mitochondrial outer membrane permeabilization is partially mediated by up-regulation of PUMA. Results shown in Fig. 4D also indicated that the amount of Bax in the cytosol fraction decreased in the presence of celecoxib but almost completely recovered to the original level by the transfection of siRNA for PUMA. These findings suggest that the celecoxib-dependent translocation of Bax from cytosol to mitochondria is mediated by the up-regulation of PUMA.

The conformational change (activation) of Bax occurs prior to Bax translocation, and seems to be required for this translocation [24]. We here monitored the conformational change of Bax by immuno-staining analysis with an antibody that specifically recognizes the active form of Bax [24]. As shown in Fig. 4E, the number of Bax (active form)-positive cells drastically increased in the presence of celecoxib, and the transfection of siRNA for PUMA returned this number to the background level, suggesting that the celecoxib-dependent activation of Bax is mediated by up-regulation of PUMA. It was recently reported that PUMA can directly bind to Bax and cause the

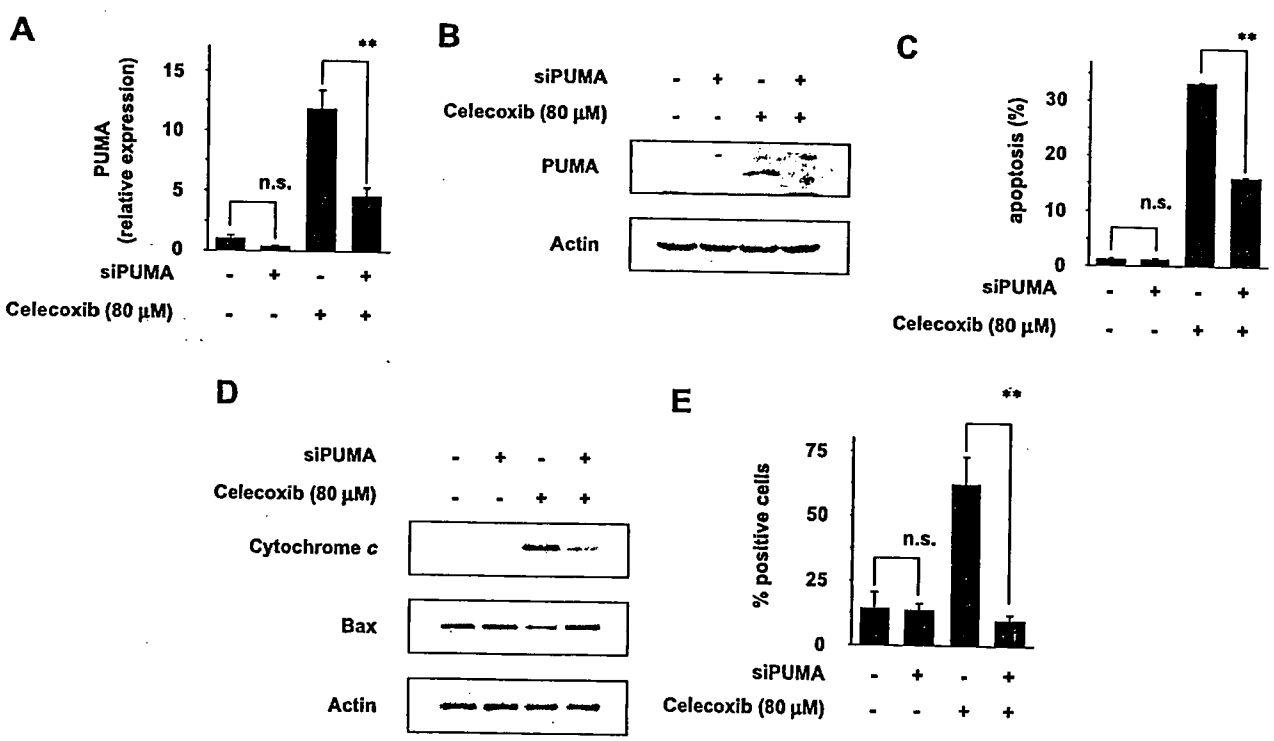

Fig. 4. Effect of siRNA for PUMA on celecoxib-induced apoptosis. AGS cells were transfected with siRNA for PUMA (siPUMA) or non-silencing siRNA. After 48 h cells were incubated with or without 80 μM celecoxib for 6 h (A), 12 h (B, D, and E) or 18 h (C). Cytosol fractions were prepared (D). The levels of *PUMA* mRNA (A), PUMA protein (B), cytochrome *c* and Bax proteins (D) were estimated by immuno-blotting or real-time RT-PCR experiments as described in the legend of Fig. 1. Apoptosis was monitored as described in the legend of Fig. 1C. Immuno-staining with the antibody against the N-terminal region of Bax (Bax N20) and DAPI-staining were performed as described in the experimental procedures. Approximately 500–700 cells were randomly counted for staining with Bax N20 (E). Values shown are means ± SD ($n = 3$–5). $^{**}P < 0.01$; n.s., not significant.

conformational change [27]. Therefore, it seems that celecoxib-induced mitochondrial dysfunction is mediated by the direct binding of PUMA to Bax, and the resulting activation and translocation of Bax. PUMA-mediated dissociation of Bax from Bcl-2 and Bcl-xl [15,17] may also be involved in the activation of Bax by PUMA, because Bcl-2 and Bcl-xl were reported to inhibit the Bax conformational change [28,29].

NSAID-induced apoptosis plays an important role not only in the anti-tumor activity of these drugs, but also in the pathology of NSAID-induced gastric ulcers, which is a major side-effect of NSAIDs in their clinical use; we recently suggested that both COX-inhibition and NSAID-induced cell death (such as apoptosis) at the gastric mucosa are necessary factors leading to the production of NSAID-induced gastric ulcers *in vivo* [30]. On this basis, we examined the molecular mechanism governing NSAID-induced apoptosis in several of our papers and found that the ER stress response (up-regulation of CHOP) and mitochondrial outer membrane permeabilization play an important role in this apoptosis [4,9,30]. In the present study, we have identified PUMA as a factor that could provide a link between the ER stress response and mitochondrial outer membrane permeabilization. In summary, the results from this study suggest that NSAID-induced apoptosis is mediated by various mechanisms, one of which is a pathway involving an increase in the intracellular Ca^{2+} level, the ER stress response, up-regulation of ATF4, up-regulation of CHOP, up-regulation of PUMA, activation and translocation of Bax and mitochondrial outer membrane permeabilization.

Acknowledgment

This work was supported by the Japan Science and Technology Agency.

References

[1] W.H. Wang, J.Q. Huang, G.F. Zheng, S.K. Lam, J. Karlberg, B.C. Wong, Non-steroidal anti-inflammatory drug use and the risk of gastric cancer: a systematic review and meta-analysis, J. Natl. Cancer Inst. 95 (2003) 1784–1791.

[2] R.A. Gupta, R.N. Dubois, Colorectal cancer prevention and treatment by inhibition of cyclooxygenase-2, Nat. Rev. Cancer 1 (2001) 11–21.

[3] S. Mima, S. Tsutsumi, H. Ushijima, M. Takeda, I. Fukuda, K. Yokomizo, K. Suzuki, K. Sano, T. Nakanishi, W. Tomisato, T. Tsuchiya, T. Mizushima, Induction of claudin-4 by nonsteroidal anti-inflammatory drugs and its contribution to their chemopreventive effect, Cancer Res. 65 (2005) 1868–1876.

[4] S. Tsutsumi, T. Gotoh, W. Tomisato, S. Mima, T. Hoshino, H.J. Hwang, H. Takenaka, T. Tsuchiya, M. Mori, T. Mizushima, Endoplasmic reticulum stress response is involved in nonsteroidal anti-inflammatory drug-induced apoptosis, Cell Death Differ. 11 (2004) 1009–1016.

[5] H. Yoshida, T. Okada, K. Haze, H. Yanagi, T. Yura, M. Negishi, K. Mori, ATF6 activated by proteolysis binds in the presence of NF-Y (CBF) directly to the cis-acting element responsible for the mammalian unfolded protein response, Mol. Cell Biol. 20 (2000) 6755–6767.

[6] S. Luo, P. Baumeister, S. Yang, S.F. Abcouwer, A.S. Lee, Induction of Grp78/BiP by translational block: activation of the Grp78 promoter by ATF4 through and upstream ATF/CRE site independent of the endoplasmic reticulum stress elements, J. Biol. Chem. 278 (2003) 37375–37385.

[7] S. Tsutsumi, T. Namba, K.I. Tanaka, Y. Arai, T. Ishihara, M. Aburaya, S. Mima, T. Hoshino, T. Mizushima, Celecoxib upregulates endoplasmic reticulum chaperones that inhibit celecoxib-induced apoptosis in human gastric cells, Oncogene 25 (2006) 1018–1029.

[8] T. Namba, T. Hoshino, K. I. Tanaka, S. Tsutsumi, T. Ishihara, S. Mima, K. Suzuki, S. Ogawa, and T. Mizushima, Up-regulation of 150-kDa oxygen-regulated protein (ORP150) by celecoxib in human gastric carcinoma cells, Mol. Pharmacol., in press.

[9] K. Tanaka, W. Tomisato, T. Hoshino, T. Ishihara, T. Namba, M. Aburaya, T. Katsu, K. Suzuki, S. Tsutsumi, T. Mizushima, Involvement of intracellular Ca2+ levels in nonsteroidal anti-inflammatory drug-induced apoptosis, J. Biol. Chem. 280 (2005) 31059–31067.

[10] W. Tomisato, K. Tanaka, T. Katsu, H. Kakuta, K. Sasaki, S. Tsutsumi, T. Hoshino, M. Aburaya, D. Li, T. Tsuchiya, K. Suzuki, K. Yokomizo, T. Mizushima, Membrane permeabilization by nonsteroidal anti-inflammatory drugs, Biochem. Biophys. Res. Commun. 323 (2004) 1032–1039.

[11] S. Cory, J.M. Adams, The Bcl2 family: regulators of the cellular life-or-death switch, Nat. Rev. Cancer 2 (2002) 647–656.

[12] A. Letai, M.C. Bassik, L.D. Walensky, M.D. Sorcinelli, S. Weiler, S.J. Korsmeyer, Distinct BH3 domains either sensitize or activate mitochondrial apoptosis, serving as prototype cancer therapeutics, Cancer Cell 2 (2002) 183–192.

[13] L. Zhang, J. Yu, B.H. Park, K.W. Kinzler, B. Vogelstein, Role of BAX in the apoptotic response to anticancer agents, Science 290 (2000) 989–992.

[14] Z. Zhang, G.H. Lai, A.E. Sirica, Celecoxib-induced apoptosis in rat cholangiocarcinoma cells mediated by Akt inactivation and Bax translocation, Hepatology 39 (2004) 1028–1037.

[15] J. Yu, L. Zhang, P.M. Hwang, K.W. Kinzler, B. Vogelstein, PUMA induces the rapid apoptosis of colorectal cancer cells, Mol. Cell 7 (2001) 673–682.

[16] K. Nakano, K.H. Vousden, PUMA, a novel proapoptotic gene, is induced by p53, Mol. Cell 7 (2001) 683–694.

[17] L. Ming, P. Wang, A. Bank, J. Yu, L. Zhang, PUMA Dissociates Bax and Bcl-X(L) to induce apoptosis in colon cancer cells, J. Biol. Chem. 281 (2006) 16034–16042.

[18] J. Yu, Z. Wang, K.W. Kinzler, B. Vogelstein, L. Zhang, PUMA mediates the apoptotic response to p53 in colorectal cancer cells, Proc. Natl. Acad. Sci. USA 100 (2003) 1931–1936.

[19] F.T. Liu, A.C. Newland, L. Jia, Bax conformational change is a crucial step for PUMA-mediated apoptosis in human leukemia, Biochem. Biophys. Res. Commun. 310 (2003) 956–962.

[20] J. Han, C. Flemington, A.B. Houghton, Z. Gu, G.P. Zambetti, R.J. Lutz, L. Zhu, T. Chittenden, Expression of bbc3, a pro-apoptotic BH3-only gene, is regulated by diverse cell death and survival signals, Proc. Natl. Acad. Sci. USA 98 (2001) 11318–11323.

[21] J. Li, B. Lee, A.S. Lee, Endoplasmic reticulum stress-induced apoptosis: multiple pathways and activation of p53-up-regulated modulator of apoptosis (PUMA) and NOXA by p53, J. Biol. Chem. 281 (2006) 7260–7270.

[22] C. Reimertz, D. Kogel, A. Rami, T. Chittenden, J.H. Prehn, Gene expression during ER stress-induced apoptosis in neurons: induction of the BH3-only protein Bbc3/PUMA and activation of the mitochondrial apoptosis pathway, J. Cell Biol. 162 (2003) 587–597.

[23] S. Tsutsumi, W. Tomisato, T. Takano, K. Rokutan, T. Tsuchiya, T. Mizushima, Gastric irritant-induced apoptosis in guinea pig gastric mucosal cells in primary culture, Biochim. Biophys. Acta 1589 (2002) 168–180.

[24] G.W. Makin, B.M. Corfe, G.J. Griffiths, A. Thistlethwaite, J.A. Hickman, C. Dive, Damage-induced Bax N-terminal change, translocation to mitochondria and formation of Bax dimers/complexes occur regardless of cell fate, EMBO J. 20 (2001) 6306–6315.

[25] G.A. FitzGerald, C. Patrono, The coxibs, selective inhibitors of cyclooxygenase-2, N. Engl. J. Med. 345 (2001) 433–442.
[26] K. Saukkonen, O. Nieminen, B. van Rees, S. Vilkki, M. Harkonen, M. Juhola, J.P. Mecklin, P. Sipponen, A. Ristimaki, Expression of cyclooxygenase-2 in dysplasia of the stomach and in intestinal-type gastric adenocarcinoma, Clin. Cancer Res. 7 (2001) 1923–1931.
[27] P.F. Cartron, T. Gallenne, G. Bougras, F. Gautier, F. Manero, P. Vusio, K. Meflah, F.M. Vallette, P. Juin, The first alpha helix of Bax plays a necessary role in its ligand-induced activation by the BH3-only proteins Bid and PUMA, Mol. Cell 16 (2004) 807–818.
[28] B. Antonsson, S. Montessuit, B. Sanchez, J.C. Martinou, Bax is present as a high molecular weight oligomer/complex in the mitochondrial membrane of apoptotic cells, J. Biol. Chem. 276 (2001) 11615–11623.
[29] A. Gross, J. Jockel, M.C. Wei, S.J. Korsmeyer, Enforced dimerization of BAX results in its translocation, mitochondrial dysfunction and apoptosis, EMBO J. 17 (1998) 3878–3885.
[30] W. Tomisato, S. Tsutsumi, T. Hoshino, H.J. Hwang, M. Mio, T. Tsuchiya, T. Mizushima, Role of direct cytotoxic effects of NSAIDs in the induction of gastric lesions, Biochem. Pharmacol. 67 (2004) 575–585.

ANALYTICAL SCIENCES MAY 2007, VOL. 23

Simultaneous Measurements of K^+ and Calcein Release from Liposomes and the Determination of Pore Size Formed in a Membrane

Takashi KATSU,*† Tomonori IMAMURA,* Keiko KOMAGOE,* Kazufumi MASUDA,* and Tohru MIZUSHIMA**

**Graduate School of Medicine, Dentistry and Pharmaceutical Sciences, Okayama University, Tsushima, Okayama 700-8530, Japan*
***Graduate School of Medical and Pharmaceutical Sciences, Kumamoto University, Oe-honmachi, Kumamoto 862-0973, Japan*

The changes induced by biologically active substances in the permeability to K^+ and calcein of liposomes composed of egg phosphatidylcholine and cholesterol were measured simultaneously in order to rapidly screen the sizes of pores formed in a membrane, using different sized markers. The substances examined in the present study were classified into three types based on differences in the rates at which K^+ and calcein were released. The first type released only K^+, and included gramicidin A. The second type predominantly released K^+, preceding the release of calcein, and included amphotericin B and nystatin. The third type, including antimicrobial peptides, such as gramicidin S, alamethicin, and melittin, and several membrane-active drugs, like celecoxib (non-steroidal anti-inflammatory drug), 1-dodecylazacycloheptan-2-one (named azone: skin permeation enhancer), and chlorpromazine (tranquilizer), caused the release of K^+ and calcein simultaneously. Thus, the sizes of pores formed in a liposomal membrane increased in the following order: types one, two, and three. We determined the size more precisely by conducting an osmotic protection experiment, measuring the release of calcein in the presence of osmotic protectants of different sizes. The radii of pores formed by the second type, amphotericin B and nystatin, were 0.36 - 0.46 nm, while the radii of pores formed by the third type were much larger, 0.63 - 0.67 nm or more. The permeability changes induced by substances of the third type are discussed in connection with a transient pore formed in a lipid packing mismatch taking place during the phase transition of dipalmitoylphosphatidylcholine liposomes.

(Received February 1, 2007; Accepted March 16, 2007; Published May 10, 2007)

Introduction

Assays of the permeability of liposomes are fundamental for investigations of the interactions between biologically active substances and membranes.[1,2] Rapid changes in the permeability of liposomal membranes can be brought about by interactions with drugs, calcium-mediated fusion, or antibody/complement-mediated lysis of antigen-bearing liposomes. Among various markers so far developed, calcein has most widely been used for such measurements.[1,3-7] Calcein fluoresces very weakly at high concentrations because of self-quenching, but its fluorescence increases at lower concentrations as quenching is reduced. Thus, the calcein entrapped inside liposomes at high concentrations is weakly fluorescent, while the calcein that has leaked out of the liposomes is highly fluorescent. Calcein-loaded liposomes have been widely used for permeability assays, because liposomal leakage can be measured *in situ* without any separation of liposomes in an assay medium.[1,3-7]

In the present study, we were particularly interested in the combination of calcein and K^+ for permeability assays and attempted to monitor simultaneously the release of calcein and K^+ from liposomes to obtain information about the sizes of pores formed in membranes. Because K^+ leakage is the first event in the permeabilization of a membrane, measurements of differences in the rates of release of K^+ and calcein, which is larger than K^+, can provide significant information about the sizes of pores made by membrane-active substances. We tested various membrane-active substances; the channel-forming peptide gramicidin A,[8,9] polyene antibiotics such as amphotericin B, nystatin, and filipin,[8,10,11] antimicrobial peptides such as gramicidin S, alamethicin, and melittin,[8,9,12-14] and membrane-disrupting drugs such as celecoxib (non-steroidal anti-inflammatory drug).[6] 1-dodecylazacycloheptan-2-one (named azone: skin permeation enhancer),[15] and chlorpromazine (tranquilizer).[16,17] Although simultaneous monitoring of the different rates of K^+ and calcein release from liposomes provided significant information about the sizes of pores generated by these substances, we further determined the sizes more precisely by conducting an osmotic protection experiment.[3,18] This experiment is based on the fact that, if the solute added to the outer medium does not pass through pores formed in the liposomal membrane, the release of calcein will not be induced because the osmotic pressure of the inner calcein is balanced with that of the solute. Thus, the sizes of pores in the membrane can be evaluated by examining whether the solutes can protect against the release of calcein. We used a series of sugars as

† To whom correspondence should be addressed.
E-mail: katsu@pharm.okayama-u.ac.jp

solutes and estimated the sizes of pores formed by the various membrane-disrupting substances described above. Furthermore, we determined the size of a pore formed transiently during the phase transition of dipalmitoylphosphatidylcholine (DPPC) liposomes to obtain further insight into the mechanism of increasing permeability induced by membrane-active substances.

Experimental

Reagents

The reagents were obtained from the following sources: calcein and sodium tetrakis[3,5-bis(trifluoromethyl)phenyl]borate (NaTFPB) were from Dojindo Laboratories (Kumamoto, Japan); egg phosphatidylcholine (PC) was from Lipid Products (Red Hill, Surry, UK); cholesterol, DPPC, amphotericin B, nystatin, filipin (as filipin complex, approximately 75% by UV spectral analysis), gramicidin S, alamethicin, melittin (from bee venom, approximately 93% by high-performance liquid chromatography), chlorpromazine hydrochloride, and valinomycin were from Sigma (St. Louis, MO, USA); gramicidin A was from Calbiochem (La Jolla, CA, USA); celecoxib was from LKT Laboratories (St. Paul, MN, USA); azone was from Koei Chemical (Osaka, Japan); bis(2-ethylhexyl) sebacate was from Fluka (Buchas, Switzerland); poly(vinyl chloride) (PVC; degree of polymerization, 1020) was from Nacalai Tesque (Kyoto, Japan); D-mannitol, sucrose, and raffinose were from Wako (Osaka, Japan); and maltotriose, maltotetraose, and maltopentaose were from Hayashibara (Okayama, Japan). All other materials were of analytical reagent grade.

Electrode system

A K^+-selective electrode was constructed using a PVC-based membrane, as reported previously.[19,20] The PVC membrane had the following composition: 1 mg of valinomycin, 10 mol% of NaTFPB relative to valinomycin, 60 µl (55 mg) of bis(2-ethylhexyl) sebacate, and PVC (30 mg). The materials were dissolved in tetrahydrofuran (about 1 ml) and poured into a flat Petri dish (28 mm in diameter). The solvent was then evaporated off at room temperature. The resulting membrane was excised and attached to a PVC tube (4 mm o.d., 3 mm i.d.) with a tetrahydrofuran adhesive. The sensor membrane was conditioned overnight in a solution of 10 mM KCl. The electrochemical cell arrangement was Ag, AgCl/internal solution/sensor membrane/sample solution//1 M NH_4NO_3 (salt bridge)//10 mM KCl/Ag, AgCl. The internal solution was the same as that used to condition the membrane. Potential measurements were made with a voltmeter produced by a field-effect transistor operational amplifier (LF356; National Semiconductor, Sunnyvale, CA, USA; input resistance $>10^{12}$ Ω) connected to a recorder. The potential values were converted to the percent release of K^+ using a previously reported equation.[21]

Preparation of liposomes

Liposomes were prepared using the reversed-phase evaporation method,[2,3,6,21] as follows. Aliquots of lipid stock solutions containing egg PC (10 µmol, 7.7 mg) and cholesterol (7.5 µmol, 2.9 mg) dissolved in chloroform/methanol (1:2, v/v) were placed in a centrifuge test tube (10 ml; Nichiden-Rika, Kobe, Japan). The solvent was evaporated using a centrifugal evaporator (RD400; Yamato, Tokyo, Japan), and the residual lipid was dried under vacuum for several hours. The lipid was then dissolved in 1.5 ml of diethyl ether, followed by the addition of 1 ml of an aqueous solution of 100 mM calcein-KOH (pH 7.4). The mixture was ultrasonicated (5201; Ohtake Works, Tokyo, Japan) at 50 W for 1 min at 0°C to obtain a homogeneous emulsion. Immediately, it was transferred to a round-bottom flask (20 ml), and the diethyl ether solvent was removed using a conventional rotary evaporator under reduced pressure (using an aspirator) at 25°C. After the diethyl ether was completely removed by passing nitrogen gas through the mixture, a homogeneous suspension of liposomes was formed. The liposomes were centrifuged (105000*g* for 15 min) and washed once with 150 mM NaCl and 10 mM NaH_2PO_4/Na_2HPO_4 (pH 7.4) to remove any untrapped calcein potassium salt. The final pellet of liposomes was suspended in 5 ml of the above-mentioned washing solution. The osmotic pressure of the inner and outer aqueous solutions was measured with an OS osmometer (Fiske, Needham, MA, USA); both were approximately 300 mOsm.

Assay procedure

The permeability was assayed at 25°C as follows. To monitor the efflux of calcein and K^+ simultaneously, the K^+ and reference electrodes were immersed in a conventional quartz cell with a light path length of 1 cm for measuring the fluorescence and set to a cuvette holder of an Ocean Optics USB2000 miniature fiber-optic spectrometer (Dunedin, FL, USA). Fiber-optic cables were connected to conduct excitation and fluorescence, and Ocean Optics OOIBase32 software was used to process the data. Figure 1 shows a device for simultaneous measurements using potentiometry and fluorometry. An aliquot of liposomal suspension (30 µl) was diluted with 1.97 ml of the following assay solution: (a) 150 mM NaCl and 10 mM NaH_2PO_4/Na_2HPO_4 (pH 7.4); (b) 180 mM mannitol, 50 mM NaCl, and 10 mM NaH_2PO_4/Na_2HPO_4 (pH 7.4); (c) 170 mM sugar containing either sucrose, raffinose, maltotriose, maltotetraose or maltopentaose, 50 mM NaCl, and 10 mM NaH_2PO_4/Na_2HPO_4 (pH 7.4). The concentration of mannitol was relatively high to make the osmotic pressure of all the solutions approximately 300 mOsm. The total volume of the liposomal suspension in the measuring cell was 2 ml, and the final phospholipid concentration was 30 µM. The suspension was constantly stirred with a stirrer bar. Subsequently, a small aliquot of a membrane-active substance was added, and incubation continued for several more minutes. Amphotericin B, nystatin, filipin, and celecoxib were dissolved in dimethyl sulfoxide; gramicidin A, gramicidin S, alamethicin, and azone were dissolved in ethanol; and melittin and chlorpromazine hydrochloride were dissolved in distilled water. The final concentrations of dimethyl sulfoxide or ethanol in assay media were less than 1% v/v. The release of calcein out of the liposomes was determined by measuring the total fluorescent intensity through a high-pass OF2-OG515 filter (pass > 515 nm; Ocean Optics) and using an USB-LS-450 LED light source module (Ocean Optics) having a maximum wavelength of 470 nm. The total amounts of calcein and K^+ in each liposome were determined after disrupting the liposomes by adding melittin (final concentration: 20 µM).[6,21] The following molecular radii of sugars were used:[22,23] mannitol, 0.36 nm; sucrose, 0.46 nm; raffinose, 0.57 nm. The apparent radii (R) of maltotriose, maltotetraose, and maltopentaose were calculated from the molecular weights (M) of the sugars using the following equation:[24]

$$R = R_{\text{raffinose}} \times \left(\frac{M}{M_{\text{raffinose}}} \right)^{1/3}.$$

$R_{\text{raffinose}} = 0.57$ nm.[22,23]

The molecular radius was thus 0.57 nm for maltotriose, 0.63 nm for maltotetraose, and 0.67 nm for maltopentaose.

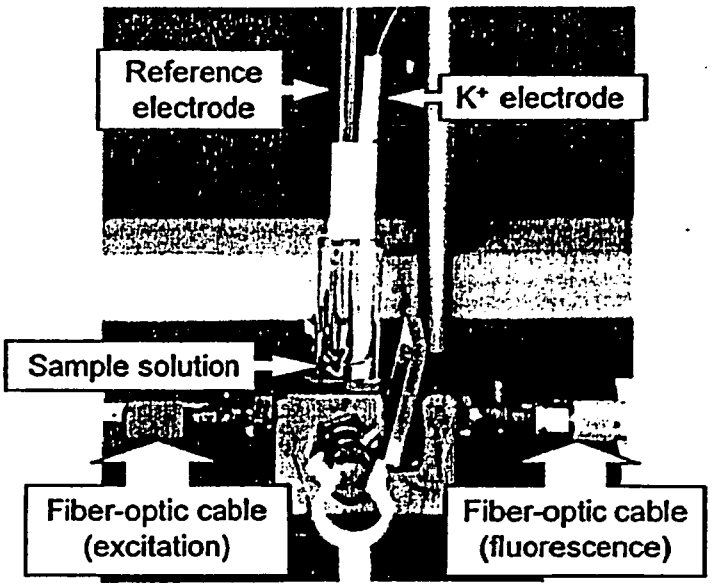

Fig. 1 Device for the simultaneous measurements of K^+ and calcein release from liposomes.

Determination of amount of calcein released from DPPC liposomes

Multilamellar liposomes composed of DPPC were prepared, using procedures similar to those described previously.[2] The dried thin film of DPPC (20 μmol, 14.7 mg) was swollen in 2 ml of 100 mM calcein-KOH (pH 7.4) at 55°C, centrifuged (22000*g* for 10 min), and washed once to remove untrapped marker. The final lipid pellet was suspended in 2 ml of 150 mM NaCl and 10 mM NaH_2PO_4/Na_2HPO_4 (pH 7.4), and an aliquot (100 μl) of this liposomal suspension was diluted with 200 μl of required assay mixture to produce a final suspension of either (a) 180 mM mannitol, 50 mM NaCl, and 10 mM NaH_2PO_4/Na_2HPO_4 (pH 7.4) or (b) 170 mM sugar containing sucrose, raffinose, maltotriose, maltotetraose or maltopentaose, 50 mM NaCl, and 10 mM NaH_2PO_4/Na_2HPO_4 (pH 7.4), as in the case of an assay examining the membrane-active substances described above. Each liposomal suspension was incubated at 35°C or 45°C for 10 min, and then centrifuged at 22000*g* for 10 min. However, in some cases, especially a suspension containing maltotetraose and maltopentaose, liposomes did not sediment and floated on the solution, because of the high density of the solution containing these sugars. We carefully pipetted the transparent part of the solution (25 μl), diluted it with 975 μl of 150 mM NaCl and 10 mM NaH_2PO_4/Na_2HPO_4 (pH 7.4), and determined the release of calcein from the liposomes by measuring the fluorescence intensity at 510 nm (excitation at 490 nm) on a Hitachi F-4500 fluorescence spectrophotometer. The fluorescence intensity corresponding to 100% release was determined by treating the liposomes ultrasonically at 60°C for 1 min using a Sibata SU-3T ultrasonic cleaner (Tokyo, Japan).

Results and Discussion

Simultaneous measurements of K^+ and calcein release

In order to directly confirm whether the combination of the K^+ electrode and fluorometry using calcein can give useful information about liposomal membrane permeability measurements, we monitored the time response of K^+ and calcein release simultaneously in a solution containing 150 mM NaCl and 10 mM NaH_2PO_4/Na_2HPO_4 (pH 7.4). We tested three typical substances: gramicidin A, amphotericin B, and gramicidin S. Gramicidin A is known to make channels specific for monovalent cations,[8,9] and amphotericin B forms a complex with cholesterol, making larger size pores in the membrane than gramicidin A.[8,10,11] Gramicidin S perturbs lipid packing, resulting in membrane permeabilization,[25] whose pore size is reported to be larger than that of amphotericin B.[18] Such differences in the sizes of pores were expected to significantly influence the time response of K^+ and calcein release. In the present experiments, we added the membrane-active substances stepwise to obtain dose-response characteristics from one experiment and, finally, melittin (20 μM) was added to determine the total amounts (100% level) of markers trapped in liposomes, as shown in Fig. 2. Equivalent amounts obtained after the addition of melittin (20 μM) and a treatment with chloroform/methanol (1:2, v/v) demonstrated that melittin caused the complete release of both markers. Gramicidin A induced only the release of K^+, demonstrating that this peptide inhibited the passage of a large molecule, calcein, forming an ion-channel passing K^+. Amphotericin B caused the release of K^+, preceding the release of calcein, while gramicidin S gave similar profiles of K^+ and calcein release, which was consistent with a previous result showing that gramicidin S formed a larger size of pore than amphotericin B.[18] Thus, the relative sizes of the pores formed in liposomal membranes can be easily compared from these experiments. It should be pointed out that the dose-response behavior of membrane-active substances can also be estimated approximately in the present assay. Figure 3 shows dose-response curves of amphotericin B and gramicidin S based on the response profiles shown in Fig. 2.

Determination of the sizes of pores

We then used the calcein-loaded liposomes to determine the sizes of pores formed in the liposomal membrane. This experiment is similar to an osmotic protection experiment using

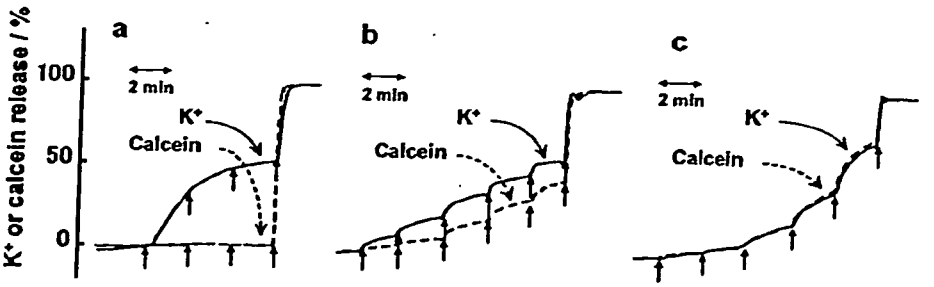

Fig. 2 K^+ and calcein release from liposomes composed of egg PC and cholesterol induced by gramicidin A (a), amphotericin B (b), and gramicidin S (c). Liposomes were suspended in a solution containing 150 mM NaCl and 10 mM NaH_2PO_4/Na_2HPO_4 (pH 7.4). The solid and dashed lines indicate traces for K^+ and calcein release, respectively. The biologically active substances were added stepwise, and the arrows indicate when. In each chart, the final arrow shows when melittin was added at a final concentration of 20 μM to induce changes in the permeability of liposomes completely. The first, second, and third arrows of (a) indicate the times of the addition of gramicidin A at final concentrations of 0.005, 0.01, and 0.02 μM, respectively. The first, second, third, fourth, and fifth arrows of (b) indicate the times of the addition of amphotericin B at final concentrations of 1, 2, 5, 10, and 20 μg ml^{-1}, respectively, while those of (c) indicate the times of the addition of gramicidin S at final concentrations of 0.1, 0.2, 0.5, 1, and 2 μM, respectively.

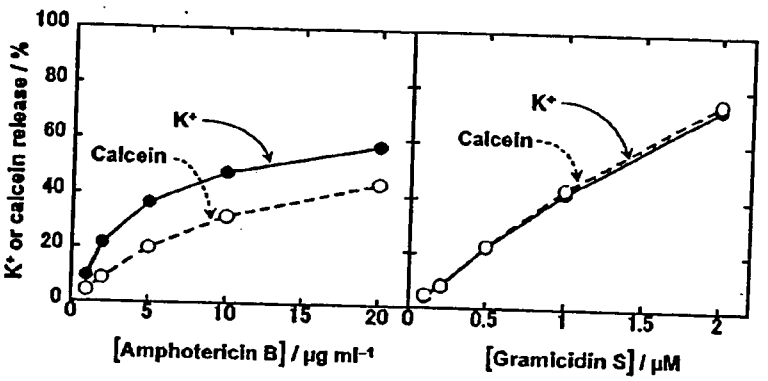

Fig. 3 Dose-response curves of K^+ and calcein release induced by amphotericin B and gramicidin S.

erythrocytes to measure the release of hemoglobin (so-called hemolysis) in the presence of a protectant.[3,18] In the erythrocyte's experiment, if the solute added to the outer medium does not pass through a channel formed in the erythrocyte's membrane, hemolysis will not be induced because the osmotic pressure of the intracellular hemoglobin is balanced by that of the solute. Thus, the size of the pore in the membrane can be evaluated by examining whether the substance added can protect against hemolysis. We applied this principle to the present liposomes and tried to determine the sizes of pores formed in liposomal membranes by amphotericin B and gramicidin S. We performed this experiment at the concentrations giving 50% calcein release, estimated from the dose-response curves shown in Fig. 3, which for amphotericin B and gramicidin S were around 20 μg ml^{-1} and 1 μM, respectively. We incubated liposomes with these substances for 5 min, because the release occurred rapidly, as shown in Fig. 2. Figure 4 shows the release of calcein induced by amphotericin B and gramicidin S as a function of the molecular radii of sugars. Amphotericin completely suppressed the release of calcein in media containing sucrose or raffinose, indicating that amphotericin B made a larger pore than mannitol (0.36 nm) and a smaller one than sucrose (0.46 nm). This result was consistent with the size of pores formed in the membranes of erythrocytes reported previously.[3,26] The protection of calcein release by gramicidin S was observed only when maltopentaose was added to the assay medium, indicating that the radius of pores was between that of maltotetraose (0.63 nm) and maltopentaose (0.67 nm). Such large pores were also observed in erythrocyte membranes.[18] These results demonstrate that the calcein-loaded liposomes can be used to estimate the size of pores formed in liposomes. It should be pointed out that the use of the present osmotic protection method is restricted to measurements of pores smaller than the molecular size of calcein (near to maltopentaose in this study). When pores exceeding the size of calcein are formed in membranes, calcein release takes place irrespective of osmotic lysis.

Application of the method using various membrane-active substances

The same experiments were performed using various membrane-active substances: polyene antibiotics (nystatin and filipin), antimicrobial peptides (alamethicin and melittin), a non-steroidal anti-inflammatory drug (celecoxib), a skin permeation enhancer (azone), and a tranquilizer (chlorpromazine). Table 1 summarizes ED_{50} values

Table 1 ED_{50} values (concentrations giving 50% K^+ or calcein release) of membrane-active substances and the sizes of pores formed in liposomes composed of egg PC/cholesterol

Type[a]	Substance	ED_{50}/μM or μg ml^{-1} [b]		Pore size/nm[c]
		K^+	Calcein	
1	Gramicidin A	0.01	> 0.2	~0.25
2	Amphotericin B	10	20	0.36 - 0.46
	Nystatin	20	50	0.36 - 0.46
3	Filipin	10	10	> 0.67
	Gramicidin S	1	1	0.63 - 0.67
	Alamethicin	10	10	> 0.67
	Melittin	0.01	0.01	0.63 - 0.67
	Celecoxib	50	50	> 0.67
	Azone	500	500	> 0.67
	Chlorpromazine	100	100	> 0.67

a. The substances are classified into three types according to differences in ED_{50} values of K^+ and calcein release as described in the text.
b. ED_{50} values were expressed in μM, except for those of polyene antibiotics (amphotericin B, nystatin, and filipin) which were expressed in μg ml^{-1}.
c. Pore sizes formed in liposomes were expressed as radii. These were determined at ED_{50} values for calcein release, except for that of gramicidin A which did not induce any calcein release up to a concentration of 0.2 μM. The pore size of gramicidin A was estimated as around the hydrated ion radius of K^+ (0.25 nm).[27]

(concentrations giving 50% K^+ or calcein release) for these substances and the sizes of pores formed in liposomes, along with those for gramicidin A, amphotericin B, and gramicidin S discussed above. As was expected, substances giving the same ED_{50} values for K^+ and calcein release (defined as type 3 in Table 1) made larger pores in the membrane. The pore sizes observed with polyene antibiotics were similar to those for erythrocytes reported previously:[3,26] that is, amphotericin B and nystatin, so-called "large polyenes",[26] formed smaller pores (type 2 in Table 1), while filipin, a so-called "small polyene",[26] made larger pores. Amphiphilic peptides, such as gramicidin S, alamethicin, and melittin, formed large pores in liposomal membranes. Although alamethicin is known to form relatively small voltage-gated ion-channels in planar lipid membranes,[8,9,14] it formed large pores in the present liposomal membrane. Melittin is known to form large pores in erythrocyte membranes,[18] consistent with this experiment. Other membrane-active drugs, azone and chlorpromazine, afforded large pores in liposomal membranes, which again supported the results of the osmotic protection experiment using human erythrocytes.[15,17]

The size of transient pores formed during the phase transition of liposomes

Then, we were interested in the mode of action of substances forming large pores. These substances are known to perturb lipid packing markedly,[6,10-15,28-31] causing a mismatch in stable lipid packing, leading to most probably transient pores in the membrane.[14] Such a mismatch in lipid packing is also observed at the interface of the fluid and ordered domain during the phase transition of phospholipids.[32,33] Thus, we determined the size of transient pores formed during the phase transition of DPPC liposomes, in order to obtain further insight into the mechanism of increases in the permeability of liposomal membrane induced by the substances defined as type 3. We measured the release of calcein in the presence of osmotic protectants below and

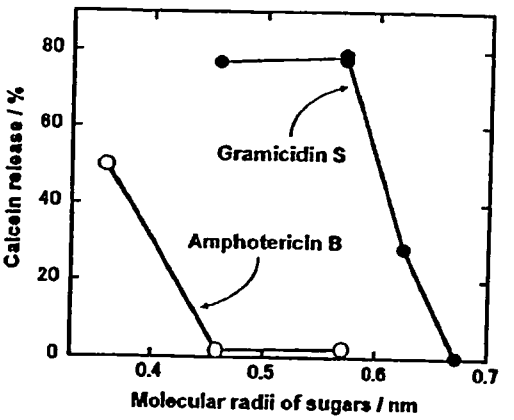

Fig. 4 Calcein release induced by amphotericin B and gramicidin S as a function of the molecular radii of sugars. The following radii were used: mannitol, 0.36 nm; sucrose, 0.46 nm; raffinose, 0.57 nm; maltotriose, 0.57 nm; maltotetraose, 0.63 nm; and maltopentaose, 0.67 nm.

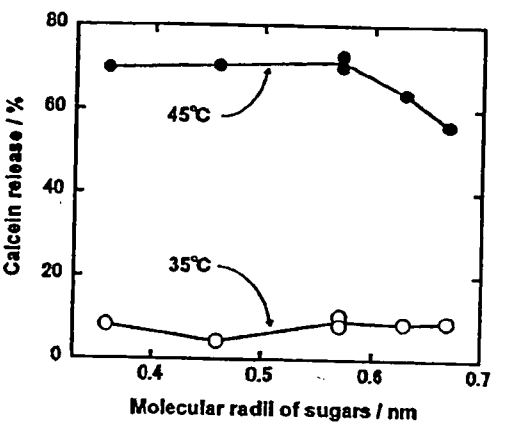

Fig. 5 Calcein release from DPPC liposomes induced with increases in temperatures (35 or 45°C) as a function of the molecular radii of sugars. The two temperatures corresponded to below and above the phase-transition temperature of DPPC liposomes (41.5°C). The molecular radii of sugars are shown in Fig. 4.

above the phase-transition temperature (41.5°C) of DPPC liposomes. In this experiment, the temperature was raised from room temperature (about 25°C) to 35 or 45°C, and thus the liposomes passed the phase transition, causing a packing mismatch in the case of 45°C. As shown in Fig. 5, the release of calcein at 35°C below the phase-transition temperature was not significant, while the case at 45°C above the phase-transition temperature was remarkable. Moreover, the release of calcein was observed even in the presence of maltopentaose, indicating that the transient pores produced during the phase transition had a radius above 0.67 nm. Such a large size was consistent with a previous result showing that the pores formed at the phase transition permitted the passage of inulin (molecular radius, 0.70 nm[23]).[34] These results support the view that the changes in permeability induced by substances of type 3 (giving large pores at ED_{50} values for calcein release) are attributable to their ability to perturb lipid packing, making an unstable domain, like a packing mismatch.

Conclusions

Simultaneous measurements of K^+ and calcein release from liposomes enabled us to predict the sizes of pores formed in membranes. These sizes could more precisely be determined by measuring the amount of calcein released in the presence of protectants of different sizes. The present method was used to analyze the sizes of pores formed by various membrane-active substances, and also those made during the phase transition of DPPC liposomes.

Acknowledgements

This work was supported by a Grant-in-Aid for Scientific Research (KAKENHI 16590027) from the Japan Society for the Promotion of Science.

References

1. R. R. C. New, in "*Liposomes: a Practical Approach*", ed. R. R. C. New, 1990, IRL Press, Oxford, 105 - 161.
2. T. Katsu, *Anal. Chem.*, 1993, *65*, 176.
3. T. Katsu, *Biol. Pharm. Bull.*, 1999, *22*, 978.
4. K. Kono and T. Takagishi, *Methods Enzymol.*, 2004, *387*, 73.
5. O. D. Hendrickson, S. N. Skopinskaya, S. P. Yarkov, A. V. Zherdev, and B. B. Dzantiev, *J. Immunoassay Immunochem.*, 2004, *25*, 279.
6. W. Tomisato, K. Tanaka, T. Katsu, H. Kakuta, K. Sasaki, S. Tsutsumi, T. Hoshino, M. Aburaya, D. Li, T. Tsuchiya, K. Suzuki, K. Yokomizo, and T. Mizushima, *Biochem. Biophys. Res. Commun.*, 2004, *323*, 1032.
7. M. Ouellet, F. Otis, N. Voyer, and M. Auger, *Biochim. Biophys. Acta*, 2006, *1758*, 1235.
8. R. B. Gennis, "*Biomembranes*", 1989, Springer-Verlag, New York.
9. B. A. Wallace, *BioEssays*, 2000, *22*, 227.
10. E. F. Gale, in "*Macrolide Antibiotics. Chemistry, Biology and Practice*", ed. S. Omura, 1984, Academic Press New York, 425 - 455.
11. J. Bolard, *Biochim. Biophys. Acta*, 1986, *864*, 257.
12. E. J. Prenner, R. N. A. H. Lewis, and R. N. McElhaney, *Biochim. Biophys. Acta*, 1999, *1462*, 201.
13. A. Tossi, L. Sandri, and A. Giangaspero, *Biopolymers*, 2000, *55*, 4.
14. Y. Shai, *Biopolymers*, 2002, *66*, 236.
15. T. Katsu, M. Kuroko, K. Sanchika, T. Morikawa, Y. Kurosaki, T. Nakayama, T. Kimura, and Y. Fujita, *Int. J. Pharm.*, 1989, *53*, 61.
16. M. Maoi, T. Suzuki, and K. Yagi, *Biochem. Pharmacol.*, 1979, *28*, 295.
17. M. R. Lieber, V. Lange, R. S. Weinstein, and T. L. Steck, *J. Biol. Chem.*, 1984, *259*, 9225.
18. T. Katsu, C. Ninomiya, M. Kuroko, H. Kobayashi, T. Hirota, and Y. Fujita, *Biochim. Biophys. Acta*, 1988, *939*, 57.
19. P. Bühlmann, E. Pretsch, and E. Bakker, *Chem. Rev.*, 1998, *98*, 1593.
20. T. Katsu, H. Kobayashi, and Y. Fujita, *Biochim. Biophys. Acta*, 1986, *860*, 608.
21. T. Katsu and K. Nakashima, *Analyst*, 1999, *124*, 883.
22. S. G. Schultz and A. K. Solomon, *J. Gen. Physiol.*, 1961, *44*, 1189.
23. R. Scherrer and P. Gerhardt, *J. Bacteriol.*, 1971, *107*, 718.
24. B. Deuticke, K. B. Heller, and C. W. M. Haest, *Biochim. Biophys. Acta*, 1986, *854*, 169.
25. T. Katsu, H. Kobayashi, T. Hirota, Y. Fujita, K. Sato, and U. Nagai, *Biochim. Biophys. Acta*, 1987, *899*, 159.
26. J. Brajtburg, G. Medoff, G. S. Kobayashi, S. Elberg, and C. Finegold, *Antimicrob. Agents Chemother.*, 1980, *18*, 586.
27. R. A. Robinson and R. H. Stokes, "*Electrolyte Solutions*", 2nd ed., 1959, Butterworths, London, 118 - 132.
28. T. Katsu, M. Kuroko, T. Morikawa, K. Sanchika, H. Yamanaka, S. Shinoda, and Y. Fujita, *Biochim. Biophys. Acta*, 1990, *1027*, 185.
29. H.-J. Freisleben, D. Blöcher, and K. Ring, *Arch. Biochem. Biophys.*, 1992, *294*, 418.
30. S. Banerjee, M. Bennouna, J. Ferreira-Marques, J. M. Ruysschaert, and J. Caspers, *J. Colloid Interface Sci.*, 1999, *219*, 168.
31. G. M. M. El Maghraby, M. Campbell, and B. C. Finnin, *Int. J. Pharm.*, 2005, *305*, 90.
32. D. Marsh, A. Watts, and P. F. Knowles, *Biochemistry*, 1976, *15*, 3570.
33. O. G. Mouritsen, K. Jørgensen, and T. Hønger, in "*Permeability and Stability of Lipid Bilayers*", ed. E. A. Disalvo and S. A. Simon, 1995, CRC, Boca Raton, 137 - 160.
34. N. Oku, S. Nojima, and K. Inoue, *Biochim. Biophys. Acta*, 1980, *595*, 277.

THE JOURNAL OF BIOLOGICAL CHEMISTRY VOL. 282, NO. 32, pp. 23240–23252, August 10, 2007

Genetic Evidence for a Protective Role for Heat Shock Factor 1 and Heat Shock Protein 70 against Colitis*

Received for publication, May 17, 2007, and in revised form, June 1, 2007 Published, JBC Papers in Press, June 7, 2007, DOI 10.1074/jbc.M704081200

Ken-Ichiro Tanaka[‡], Takushi Namba[‡], Yasuhiro Arai[‡], Mitsuaki Fujimoto[§], Hiroaki Adachi[¶], Gen Sobue[¶], Koji Takeuchi[‖], Akira Nakai[§], and Tohru Mizushima[‡1]

From the [‡]Graduate School of Medical and Pharmaceutical Sciences, Kumamoto University, Kumamoto 862-0973, Japan, the [§]Yamaguchi University School of Medicine, Yamaguchi 755-8505, Japan, the [¶]Nagoya University Graduate School of Medicine, Nagoya 466-8550, Japan, and the [‖]Kyoto Pharmaceutical University, Kyoto 607-8414, Japan

Inflammatory bowel disease (IBD) involves infiltration of leukocytes into intestinal tissue, resulting in intestinal damage induced by reactive oxygen species (ROS). Pro-inflammatory cytokines and cell adhesion molecules (CAMs) play important roles in this infiltration of leukocytes. The roles of heat shock factor 1 (HSF1) and heat shock proteins (HSPs) in the development of IBD are unclear. In this study, we examined the roles of HSF1 and HSPs in an animal model of IBD, dextran sulfate sodium (DSS)-induced colitis. The colitis worsened or was ameliorated in HSF1-null mice or transgenic mice expressing HSP70 (or HSF1), respectively. Administration of DSS up-regulated the expression of HSP70 in colonic tissues in an HSF1-dependent manner. Expression of pro-inflammatory cytokines and CAMs and the level of cell death observed in colonic tissues were increased or decreased in DSS-treated HSF1-null mice or transgenic mice expressing HSP70, respectively, relative to control wild-type mice. Relative to macrophages from control wild-type mice, macrophages prepared from HSF1-null mice or transgenic mice expressing HSP70 displayed enhanced or reduced activity, respectively, for the generation of pro-inflammatory cytokines in response to lipopolysaccharide stimulation. Suppression of HSF1 or HSP70 expression *in vitro* stimulated lipopolysaccharide-induced up-regulation of CAMs or ROS-induced cell death, respectively. This study provides the first genetic evidence that HSF1 and HSP70 play a role in protecting against DSS-induced colitis. Furthermore, this protective role seems to involve various mechanisms, such as suppression of expression of pro-inflammatory cytokines and CAMs and ROS-induced cell death.

Inflammatory bowel disease (IBD),[2] Crohn disease, and ulcerative colitis have become substantial health problems with an actual prevalence of 200–500 cases/100,000 people in western countries, which almost double every 10 years (1). Although the etiology of IBD is not yet fully understood, recent studies suggest that IBD involves chronic inflammatory disorders in the intestine because of "a vicious cycle." Infiltration into intestinal tissues causes intestinal mucosal damage induced by reactive oxygen species (ROS) that are released from the activated leukocytes, and this intestinal mucosal damage further stimulates the infiltration of leukocytes (2). To understand the molecular mechanism underlying the pathogenesis of IBD and to develop new types of clinical drugs for IBD, identification of endogenous factors that positively or negatively affect the development of IBD is important. For this purpose, various experimental animal colitis models, in particular the dextran sulfate sodium (DSS)- and trinitrobenzenesulfonic acid-induced colitis models, have been used (3).

Pro-inflammatory cytokines play an important role in the activation and infiltration of leukocytes that are associated with IBD. This conclusion is supported by a range of evidence. Increases in the levels of various pro-inflammatory cytokines (such as tumor necrosis factor-α (TNF-α), interleukin (IL)-1β, and IL-6) in intestinal tissues has been reported in both IBD patients and animal models of IBD (4, 5). TNF-α-deficient mice or transgenic mice with enhanced production of TNF-α show a phenotype of resistance to trinitrobenzenesulfonic acid-induced colitis or the spontaneous development of an IBD-like disorder, respectively (6, 7). A chimeric monoclonal antibody against TNF-α, infliximab, is effective for the treatment of Crohn disease patients (6, 8). Because TNF-α secondarily stimulates the production of many other pro-inflammatory cytokines (9), TNF-α is thought to play a crucial role in the pathogenesis of IBD.

Cell adhesion molecules (CAMs) also play an important role in the infiltration of leukocytes associated with IBD, as is suggested by the following evidence. CAMs expressed on vascular endothelial cells (such as intercellular adhesion molecule-1 (ICAM-1) and vascular cell adhesion molecule-1 (VCAM-1)) bind to counterparts expressed on leukocytes, and this binding is an essential step in the recruitment of blood circulating leukocytes into inflamed tissues (10). Up-regulation of the expression of various CAMs, including VCAM-1and ICAM-1, in intestinal tissues in both IBD patients and animal models of IBD has been reported (10, 11). Immunoneutralization of VCAM-1 significantly sup-

* This work was supported by grants-in-aid for scientific research from the Ministry of Health, Labor, and Welfare of Japan. The costs of publication of this article were defrayed in part by the payment of page charges. This article must therefore be hereby marked "*advertisement*" in accordance with 18 U.S.C. Section 1734 solely to indicate this fact.

[1] To whom correspondence should be addressed. Tel. and Fax: 81-96-371-4323; E-mail: mizu@gpo.kumamoto-u.ac.jp.

[2] The abbreviations used are: IBD, inflammatory bowel disease; ROS, reactive oxygen species; DSS, dextran sulfate sodium; TNF-α, tumor necrosis factor-α; IL, interleukin; CAMs, cell adhesion molecules; ICAM-1, intercellular adhesion molecule-1; VCAM-1, vascular cell adhesion molecule-1; HSPs, heat shock proteins; HSF1, heat shock factor 1; LPS, lipopolysaccharide; DAI, disease activity index; TBARS, thiobarbituric acid-reactive substance(s); VLA-4, very late antigen-4; MAdCAM-1, mucosal addressin cell adhesion molecule-1; siRNA, small interfering RNA; TUNEL, terminal deoxynucleotidyltransferase-mediated biotinylated UTP nick end labeling.

presses trinitrobenzenesulfonic acid-induced colitis (12), whereas ICAM-1-deficient mice show a phenotype of resistance to DSS-induced colitis (13).

Heat shock proteins (HSPs) are induced by various stressors (such as ROS) to provide cellular resistance to these stressors (14–16). This up-regulation of HSP expression by stressors is achieved at the level of transcription through a consensus *cis*-element (heat shock element) and a transcription factor (heat shock factor 1 (HSF1)) that specifically binds to a heat shock element located upstream of the *hsp* genes (17). An essential role for HSF1 in the stressor-induced up-regulation of HSPs was demonstrated by the observation that disruption to the activity of HSF1 leads to the loss of stressor-induced HSP up-regulation (17, 18). HSPs and HSF1 also have attracted considerable attention as candidates for endogenous factors that affect the development of IBD because some HSPs, including HSP70, were reported to be overexpressed in the intestinal tissues of IBD patients and in an animal model of IBD (19–23). HSF1 negatively regulates the expression of TNF-α and IL-1β genes (24, 25). The expression of copper/zinc superoxide dismutase-1, which is protective against IBD, is positively regulated by HSF1 (26, 27). All these previous results suggest that HSPs and HSF1 have negative roles in the development of IBD (*i.e.* protective roles against IBD); however, there is no direct evidence (such as genetic evidence) to support this idea. Furthermore, there are some data that suggest positive roles for HSPs and HSF1 in the development of IBD: HSF1 positively regulates expression of the IL-6 gene; extracellular HSPs elicit an inflammatory response; and autoantibodies and reactive T-cells against HSPs have been found in IBD patients (28–31). Therefore, the effects of genetic alteration of HSPs and HSF1 on the development of colitis in animal models of IBD should be examined to understand the exact role (positive or negative) of HSPs and HSF1 in IBD. In this study, we used HSF1-null mice and transgenic mice expressing HSP70 or HSF1 to examine the role of HSF1 and HSPs in the pathogenesis of DSS-induced colitis. The results clearly show that HSF1 and HSP70 contribute to the protection of colonic tissues against DSS-induced colitis. Furthermore, the results suggest that HSF1 and HSP70 achieve this protective role though various mechanisms, such as inhibition of intestinal mucosal cell death induced by ROS and suppression of DSS-induced expression of pro-inflammatory cytokines, including TNF-α, and CAMs in intestinal tissues.

EXPERIMENTAL PROCEDURES

Chemicals and Animals—Paraformaldehyde, 3-(4,5-dimethylthiazol-2-yl)-2,5-diphenyltetrazolium bromide, menadione, peroxidase standard, fetal bovine serum, *o*-dianisidine, and hexadecyltrimethylammonium bromide were obtained from Sigma. Thiobarbituric acid, butylated hydroxytoluene, 1-butanol, and pyridine were from Nacalai Tesque, Inc. (Kyoto, Japan). DSS (M_r 5000, 15–20% sulfur content) was from Wako Pure Chemical Industries, Ltd. (Tokyo, Japan). Proteose peptone was from BD Biosciences. Lipopolysaccharide (LPS) was from List Biological Laboratories, Inc. (Campbell, CA). Enzyme-linked immunosorbent assay kits for TNF-α, IL-1β, and IL-6 were from Pierce. Optimal cutting temperature compound was from Sakura Finetek (Tokyo). Mayer's hematoxylin, 1% eosin alcohol solution, and malinol were from Muto Pure Chemicals (Tokyo). Terminal nucleotidyltransferase was obtained from Toyobo Co., Ltd. (Osaka, Japan). The Envision kit was from Dako (Carpinteria, CA). Biotin-14-ATP and Alexa Fluor 488-conjugated streptavidin were purchased from Invitrogen. VECTASHIELD was from Vector Laboratories (Burlingame, CA). 4′,6-Diamidino-2-phenylindole was from Dojindo Laboratories (Kumamoto, Japan). The RNeasy kit and HiPerFect were obtained from Qiagen Inc. (Valencia, CA); the first-strand cDNA synthesis kit was from GE Healthcare (Little Chalfont, Buckinghamshire, UK); and iQ SYBR Green Supermix was from Bio-Rad. HCT-15 cells were obtained from the Cell Resource Center for Biochemical Research at Tohoku University (Sendai, Japan). bEnd.3 (mouse brain endothelioma) cells were from American Type Culture Collection (Manassas, VA). HSF1-null mice, transgenic mice expressing HSF1, and their respective wild-type mice (8–10 weeks old) were prepared as described previously (31, 32). Transgenic mice expressing HSP70 and their wild-type counterparts (8–10 weeks old) were gifts from Drs. C. E. Angelidis and G. N. Pagoulatos (University of Ioannina, Ioannina, Greece) and were prepared as described previously (33). Homozygotic transgenic mice expressing HSP70 and heterozygotic transgenic mice expressing HSF1 were used in experiments.

Development of DSS-induced Colitis and Measurement of Colon Length and the Disease Activity Index (DAI)—Colitis was induced in mice by the addition of 3% (w/v) DSS (final concentration) to their drinking water. The animals were allowed free access to the DSS-containing water for 7 days. After 7 days, the animals were placed under deep ether anesthesia and killed; the colons were dissected and measured from the ileocecal junction to the anal verge.

The DAI was determined macroscopically by an observer unaware of the treatment the mice had received according to previously reported criteria (34). Briefly, the DAI was calculated as the sum of the diarrheal stool score (0, normal stool; 1, mildly soft stool; 2, very soft stool; and 3, watery stool) and the bloody stool score (0, normal color stool; 1, brown color stool; 2, reddish color stool; and 3, bloody stool).

Myeloperoxidase Activity—Myeloperoxidase activity in the colonic tissues was measured as described previously (35, 36). After 7 days of DSS treatment, animals were placed under deep ether anesthesia and killed. Colons were dissected, rinsed with cold saline, and cut into small pieces. Samples were homogenized in 50 mM phosphate buffer, freeze-thawed, and centrifuged. The protein concentrations of the supernatants were determined using the Bradford method (37). Myeloperoxidase activity was determined in 10 mM phosphate buffer with 0.5 mM *o*-dianisidine, 0.00005% (w/v) hydrogen peroxide, and 20 μg of protein. Myeloperoxidase activity was obtained from the slope of the reaction curve, and its specific activity was expressed as the number of hydrogen peroxide molecules converted per min/mg of protein.

Lipid Peroxidation Measured by Thiobarbituric Acid-reactive Substances (TBARS)—The amounts of TBARS in the colonic tissues were measured as described previously (35, 38). After 7 days of DSS treatment, animals were placed under deep ether anesthesia and killed. Colons were dissected, rinsed with cold saline, cut into small pieces, and weighed. Samples were homogenized in 1.15% KCl solution and centrifuged. Supernatants were mixed with 20 μl of 8.1% SDS solution, 150 μl of 20% acetic acid solution, and 5 μl of 0.8% butylated hydroxytoluene solution; shaken vigorously for 1 min; mixed with 150 μl of 0.8% thiobarbituric acid solution; shaken vigorously for 1 min; and finally boiled for 1 h. Samples were mixed with 500 μl of 1-butanol and pyridine (15:1), shaken vigorously for 1 min, and centrifuged. The absorbance of the supernatant was measured at 532 nm, and the amount of TBARS was expressed as the number of TBARS molecules/g of tissue.

Real-time Reverse Transcription-PCR Analysis—Total RNA was extracted from colonic tissues using the RNeasy kit according to the manufacturer's protocol. Samples (2.5 μg of RNA) were reverse-transcribed using the first-strand cDNA synthesis kit according to the manufacturer's instructions. Synthesized cDNA was used in real-time reverse transcription-PCR (Chromo 4 system, Bio-Rad) experiments using iQ SYBR Green Supermix and analyzed with Opticon Monitor software according to the manufacturer's instructions. The real-time PCR cycle conditions were 50 °C for 2 min, followed by 90 °C for 10 min, and finally 45 cycles at 95 °C for 30 s and at 63 °C for 60 s. Specificity was confirmed by electrophoretic analysis of the reaction products and by inclusion of template- or reverse transcriptase-free controls. To normalize the amount of total RNA present in each reaction, glyceraldehyde-3-phosphate dehydrogenase or actin cDNA was used as an internal standard.

Primers were designed using the Primer3 website (frodo.wi.mit.edu/cgi-bin/primer3/primer3_www.cgi). The primers used for detection of mouse cDNA included the following: *hsp25*, 5′-cctcttccctatcccctgag-3′ (forward) and 5′-ttggctccagactgttcaga-3′ (reverse); *hsp60*, 5′-cgttgccaataacacaaacg-3′ (forward) and 5′-cttcaggggttgtcacaggt-3′ (reverse); *hsp70*, 5′-tggtgctgacgaagatgaag-3′ (forward) and 5′-aggtcgaagatgagcacgtt-3′ (reverse); TNF-α, 5′-cgtcagccgatttgctatct-3′ (forward) and 5′-cggactccgcaaagtctaag-3′ (reverse); IL-1β, 5′-gatcccaagcaataccccaaa-3′ (forward) and 5′-ggggaactctgcagactcaa-3′ (reverse); IL-6, 5′-ctggagtcacagaaggagtgg-3′ (forward) and 5′-ggtttgccgagtagatctcaa-3′ (reverse); superoxide dismutase-1, 5′-ccagtgcaggacctcatttt-3′ (forward) and 5′-ttgtttctcatggaccacca-3′ (reverse); very late antigen-4 (*vla-4*), 5′-cagagccacacccaaaagtt-3′ (forward) and 5′-tgaaatgtcgtttgggtcttt-3′ (reverse); *mac-1*, 5′-tgtgagcagcactgagatcc-3′ (forward) and 5′-atggctccactttggtctct-3′ (reverse); L-selectin, 5′-attcctgtagccgtcatggt-3′ (forward) and 5′-catcctttcttgagatttcttgc-3′ (reverse); *vcam-1*, 5′-ctcctgcacttgtggaaatg-3′ (forward) and 5′-tgtacgagccatccacagac-3′ (reverse); *icam-1*, 5′-tcgtgatggcagcctcttat-3′ (forward) and 5′-gggcttgtcccttgagtttt-3′ (reverse); mucosal addressin cell adhesion molecule-1 (*madcam-1*), 5′-gcaggctgggagctactct-3′ (forward) and 5′-tccctcttgtggtaggttgc-3′ (reverse); and *hsf1*, 5′-tgctggacattcaggagctt-3′ (forward) and 5′-tgtagtgcaccagctgcttt-3′ (reverse). The primers used for detection of human cDNA included the following: *HSP70*, 5′-aggccaacaagatcaccatc-3′ (forward) and 5′-tcgtcctccgctttgtactt-3′ (reverse); and *HSF1*, 5′-gaaaagtgcctcagcgtagc-3′ (forward) and 5′-ctcagcatggtctgcaggt-3′ (reverse).

Histological and Immunohistochemical Analyses—Colonic tissue samples were fixed in 4% buffered paraformaldehyde, embedded in optimal cutting temperature compound, and cryosectioned. For histological examination (hematoxylin and eosin staining), sections were stained first with Mayer's hematoxylin and then with 1% eosin alcohol solution. Samples were mounted with malinol and inspected using an Olympus IX70 or BX51 microscope. For histological evaluation of the tissue damage (damage score) and areas of lesions (extent of lesion), sections were evaluated microscopically by an observer unaware of the treatment the animals had received and quantified as described (39, 40). Colonic damage was categorized into 6 groups (0, normal mucosa; 1, infiltration of inflammatory cells; 2, shortening of the crypt by <50%; 3, shortening of the crypt by >50%; 4, crypt loss; and 5, destruction of epithelial cells (ulceration and erosion)). The extent of lesions in the total colon was categorized into six grades (0, 0%; 1, 1–20%; 2, 21–40%; 3, 41–60%; 4, 61–80%; and 5, 81–100%).

For immunohistochemical analysis, sections were treated in a microwave oven with 0.01 M citric acid buffer for antigen activation and incubated with 0.3% hydrogen peroxide in methanol for removal of endogenous peroxidase. Sections were blocked with 2.5% goat serum for 10 min, incubated for 12 h with antibody against HSP70 (1:200 dilution) in the presence of 2.5% bovine serum albumin, and then incubated for 1 h with peroxidase-labeled polymer conjugated to goat anti-mouse immunoglobulins. 3,3′-Diaminobenzidine was applied to the sections, which were then incubated with Mayer's hematoxylin. Samples were mounted with malinol and inspected using an Olympus IX70 or BX51 fluorescence microscope.

Small Interfering RNA (siRNA) Targeting of Genes—The HSF1- and HSP70-specific siRNAs were purchased from Qiagen Inc. HCT-15 and bEnd.3 cells were transfected with siRNA using HiPerFect transfection reagent according to the manufacturer's instructions. Non-silencing siRNA (5′-uucuccgaacgugucacgudTdT-3′ and 5′-acgugacacguucggagaadTdT-3′) was used as a negative control.

Preparation of Mouse Peritoneal Macrophages and Enzyme-linked Immunosorbent Assay—Mouse peritoneal macrophages were prepared as described previously (41). Mice were given 2 ml of 10% proteose peptone by intraperitoneal injection, and peritoneal cells were harvested 3 days later. The cells were seeded in 35-mm culture dishes at 1×10^6 cells/dish in RPMI 1640 medium supplemented with 10% heat-inactivated fetal bovine serum. After incubation for 4 h, non-adherent cells were removed, and adherent cells were cultured for use in the experiments. Virtually all of the adherent cells were macrophages, as described previously (41). The amounts of pro-inflammatory cytokines secreted into the medium were measured by enzyme-linked immunosorbent assay according to the manufacturer's protocol.

Terminal Deoxynucleotidyltransferase-mediated Biotinylated UTP Nick End Labeling (TUNEL) Assay—Colonic tissue samples were fixed in 4% buffered paraformaldehyde, embedded in optimal cutting temperature compound, and cryosectioned. Sections were incubated first with proteinase K (20 μg/ml) for 15 min at 37 °C, then with terminal nucleotidyltransferase and biotin-14-ATP for 1 h at 37 °C, and finally with Alexa Fluor 488-conjugated streptavidin and 4′,6-diamidino-2-phenylindole (5 μg/ml) for 2 h. Samples were mounted with VECTASHIELD and inspected using an Olympus IX70 or BX51 fluorescence microscope.

Statistical Analysis—All values are expressed as the mean ± S.E. Two-way analysis of variance, followed by Scheffe's multiple comparison test or Tukey's test, was used to evaluate differences between groups. Student's *t* test for unpaired results was used to evaluate differences between two groups. Differences were considered to be significant for *p* values <0.05.

RESULTS

DSS-induced Colitis and Expression of HSPs in HSF1-null Mice—The severity of DSS-induced colitis can be monitored by various indexes, such as body weight, DAI, colon length, myeloperoxidase activity, TBARS amount, and histological indexes. We compared the time course of development of colitis induced by 3% DSS administration in HSF1-null mice and wild-type mice (ICR) by monitoring body weight and the DAI. Administration of 3% DSS caused a mild increase in the DAI, but did not affect the body weight of the wild-type mice. In contrast, administration of 3% DSS resulted in a higher DAI score and loss of body weight in HSF1-null mice (Fig. 1, *A* and *B*). DSS-induced colon shortening, used as a morphometric measure for the degree of inflammation, was more severe in HSF1-null mice than in wild-

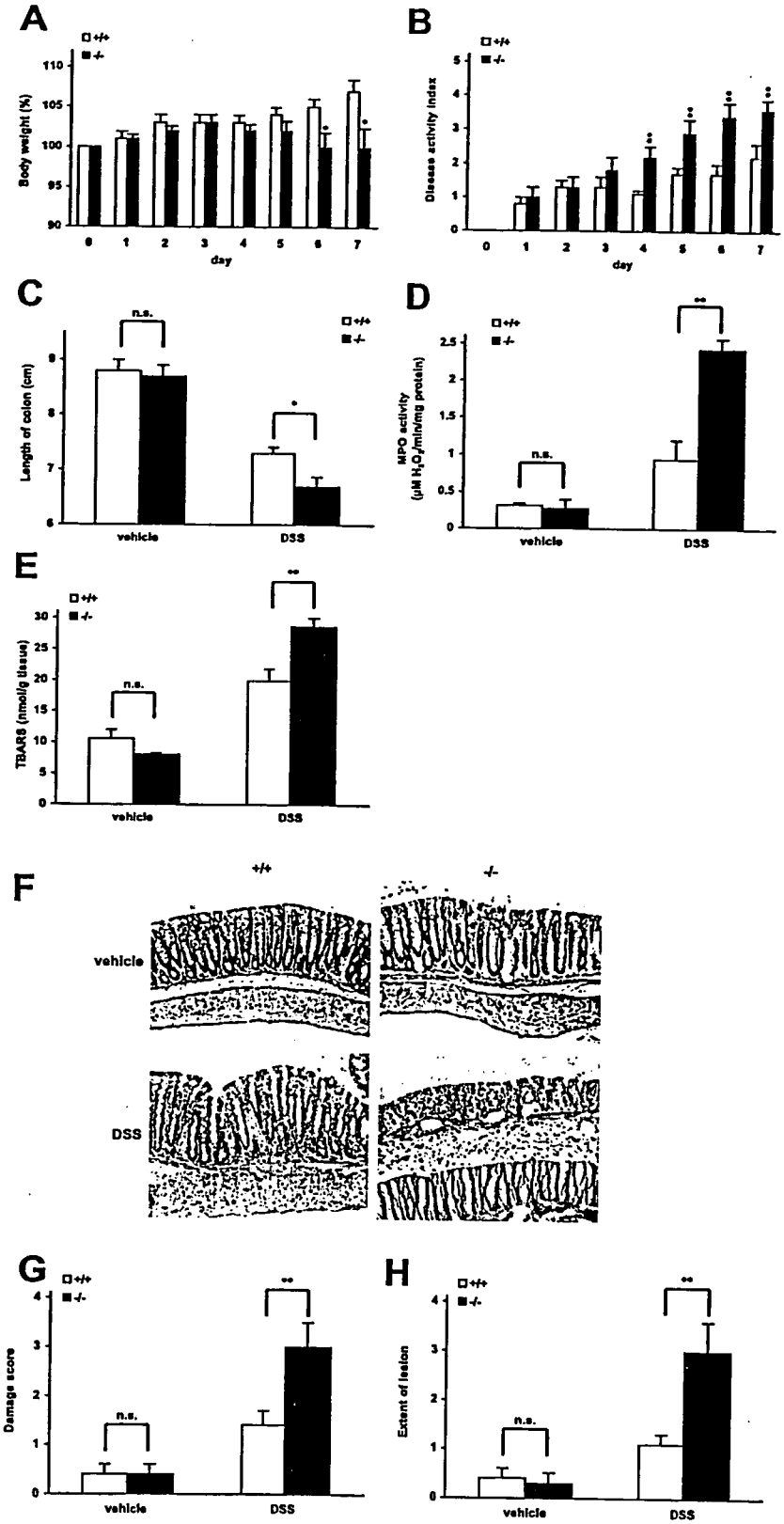

FIGURE 1. **Development of DSS-induced colitis in HSF1-null and wild-type mice.** HSF1-null mice (−/−) and wild-type mice (+/+; ICR) were treated with or without 3% DSS for 7 days. Body weight (*A*) and the DAI (*B*) were measured daily. After 7 days, colon length (*C*), colonic myeloperoxidase (*MPO*) activity (*D*), and colonic TBARS (*E*) were determined as described under "Experimental Procedures." After 7 days, sections of colonic tissues were prepared and subjected to histological examination (hematoxylin and eosin staining), and the damage score and extent of lesion for eight independent sections were determined (*G* and *H*). One of the sections is shown (*F*). Values are the mean ± S.E. ($n = 3$–10). *, $p < 0.05$; **, $p < 0.01$; *n.s.*, not significant.

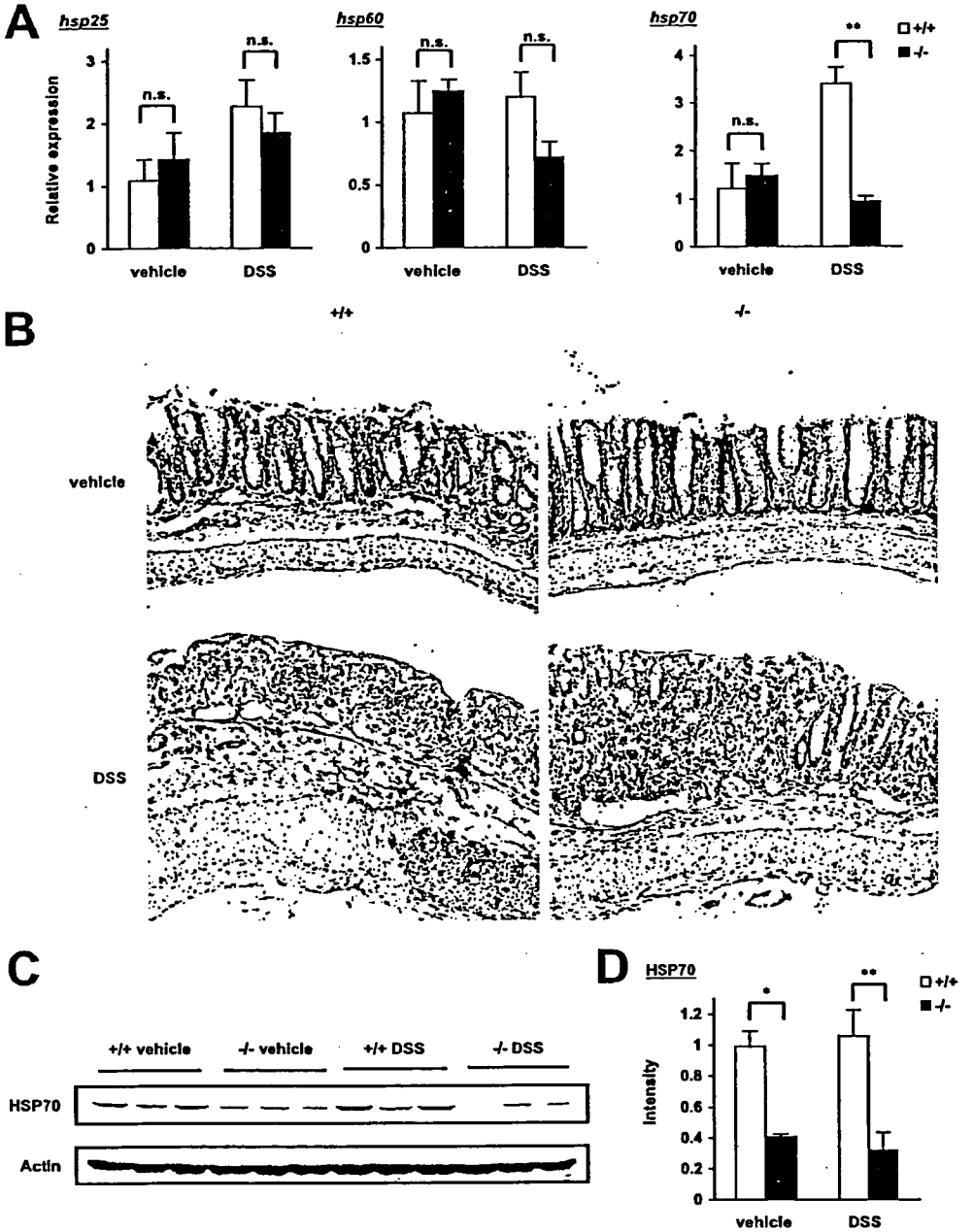

FIGURE 2. **Expression of HSPs in colonic tissues of HSF1-null and wild-type mice.** *A*, HSF1-null mice (−/−) and wild-type mice (ICR) (+/+) were treated with or without 3% DSS for 7 days (*A–D*). Colonic tissues were removed, and total RNA was extracted. Samples were subjected to real-time reverse transcription-PCR, using a specific primer set for each gene. Values were normalized to the *GAPDH* gene, expressed relative to the control sample (i.e. wild-type mice without DSS treatment), and are given as the mean ± S.E. ($n = 3–6$). **, $p < 0.01$. n.s., not significant. *B*, sections of colonic tissues were prepared and subjected to immunohistochemical analysis with an antibody against HSP70. *C*, whole cell extracts were analyzed by immunoblotting with an antibody against HSP70 or actin. *D*, the band intensity of HSP70 was determined by densitometric scanning. Gel-loading levels were compensated against the band intensity of actin, expressed relative to the control sample, and are given as the mean ± S.E. ($n = 3$). **, $p < 0.01$; *, $p < 0.05$.

type mice (Fig. 1*C*). Colonic myeloperoxidase activity, an indicator of leukocyte infiltration, was much higher in DSS-administered HSF1-null mice than in wild-type mice (Fig. 1*D*). Colonic TBARS, an index of lipid peroxidation associated with inflammation, was also higher in DSS-administered HSF1-null mice than in wild-type mice (Fig. 1*E*). Fig. 1*F* shows the results of histological analysis of colonic tissues prepared from DSS-administered and untreated HSF1-null and wild-type mice. More extensive crypt loss, epithelial destruction, and leukocyte infiltration were observed in sections from DSS-administered HSF1-null mice than in those from wild-type mice. Histological score analysis revealed that the histological differences were statistically significant (Fig. 1, *G* and *H*). The results in Fig. 1 show that HSF1-null mice are more sensitive to DSS-induced colitis than their wild-type counterparts.

We monitored the expression of *hsp* mRNAs in the colonic tissues of DSS-administered and untreated HSF1-null and wild-type mice by real-time reverse transcription-PCR. The expression of *hsp70* (but not *hsp25* or *hsp60*) mRNA was significantly lower in DSS-treated HSF1-null mice than in wild-type mice (Fig. 2*A*). DSS administration clearly up-regulated the expression of *hsp70* mRNA (Fig. 2*A*). On the basis of these results, we subsequently focused on HSP70.

Immunohistochemical analysis demonstrated that DSS administration increased the levels of HSP70 in colonic mucosa and around colonic vessels in wild-type mice, but not in HSF1-null mice (Fig. 2*B*). Fig. 2 (*C* and *D*) shows the protein level of HSP70 as assessed by the immunoblotting assay. The level of HSP70 was clearly lower in DSS-administered HSF1-null mice than in wild-type mice. The results also show that DSS administration did not clearly increase the amount of HSP70, which is inconsistent with the results in Fig. 2*B*. This may be because total colonic tissues or only damaged tissues were used for immunoblotting or immunohistochemical analysis, respectively. On the basis of the results in Fig. 2, we consider that that the inability of HSF1-null mice to induce synthesis of HSP70 is responsible for their phenotypic sensitivity to DSS-induced colitis (Fig. 1).

DSS-induced Colitis in Transgenic Mice Expressing HSF1 or HSP70—The development of DSS-induced colitis in transgenic mice expressing HSF1 and wild-type mice (C57/BL6) was compared (Fig. 3). As shown in Fig. 3 (*A* and *B*), trans-

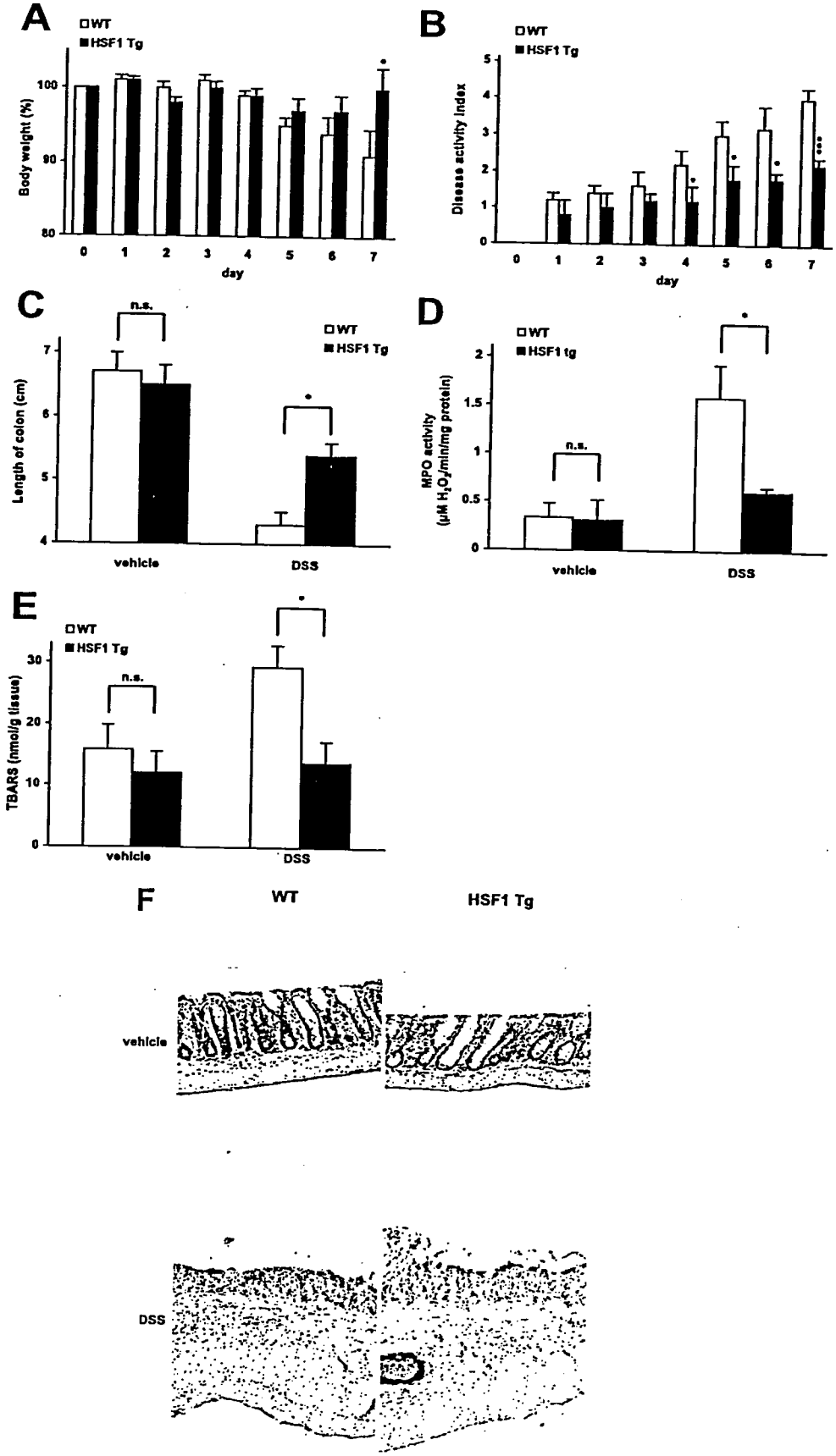

FIGURE 3. **Development of DSS-induced colitis in transgenic mice expressing HSF1 and wild-type mice.** Development of DSS-induced colitis was induced and monitored in transgenic mice expressing HSF1 (*HSF1 Tg*) and wild-type mice (*WT*; C57/BL6) as described in the legend of Fig. 1 (*A–E*). Values are the mean ± S.E. (n = 3–5). *MPO*, myeloperoxidase. *, $p < 0.05$; ***, $p < 0.001$; *n.s.*, not significant. The expression of HSP70 in colonic tissues was monitored by immunohistochemical analysis as described in the legend of Fig. 2 (*F*).

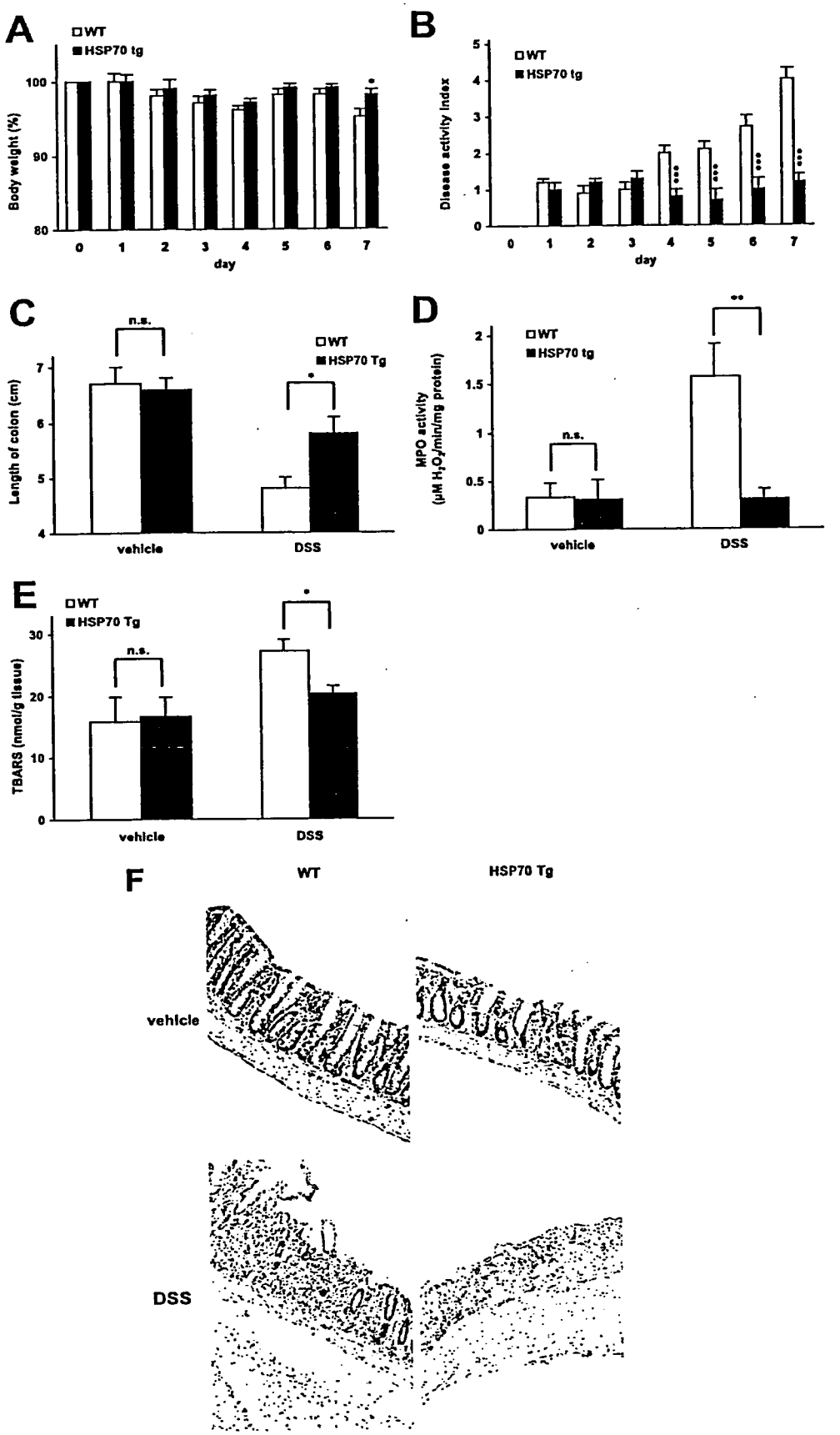

FIGURE 4. **Development of DSS-induced colitis in transgenic mice expressing HSP70 and wild-type mice.** DSS-induced colitis was induced and monitored in transgenic mice expressing HSP70 (*HSP70 Tg*) and wild-type mice (*WT*; C57/BL6) as described in the legend of Fig. 1 (*A–E*). Values are the mean ± S.E. (n = 3–10). *MPO*, myeloperoxidase. *, $p < 0.05$; **, $p < 0.01$; ***, $p < 0.001$; *n.s.*, not significant. The expression of HSP70 in colonic tissues was monitored by immunohistochemical analysis as described in the legend of Fig. 2 (*F*).

genic mice expressing HSF1 were more resistant than wild-type mice to DSS-dependent loss of body weight and increase in the DAI. The differences in the extent of DSS-induced colitis in the two groups of wild-type mice (shown in Figs. 1 and 3) must be due to their different genetic backgrounds (ICR and C57/BL6). Judging from other indexes of colitis (colon length, colonic myeloperoxidase activity and colonic TBARS), it is obvious that transgenic mice expressing HSF1 developed less DSS-induced colitis than their wild-type counterparts (Fig. 3, *C–E*). Immunohistochemical analysis demonstrated that HSP70 staining was more obvious in the colonic tissues of transgenic mice compared with wild-type mice with or without DSS treatment (Fig. 3*F*). This implies that the higher expression of HSP70 in the transgenic mouse relative to the wild-type mouse is responsible for its phenotype of resistance to DSS-induced colitis. The tissue section in Fig. 3*F* shows significant colitis even in transgenic mice expressing HSF1. This is because induction of HSP70 is clear around lesions; thus, we present the section prepared from tissues around lesions. When we performed histological score analysis (as in Fig. 1, *G* and *H*), the results showed that both colonic damage and the extent of lesions were lower in transgenic mice expressing HSF1 than in wild-type mice (data not shown).

To test this idea, the development of DSS-induced colitis was compared in transgenic mice expressing HSP70 and their wild-type counterparts (C57/BL6) (Fig. 4). Although there was no clear difference in DSS-dependent loss of body weight in the two groups (Fig. 4*A*), a DSS-dependent increase in the DAI was clearly suppressed in transgenic mice expressing HSP70 compared with wild-type mice (Fig. 4*B*). All of the other indexes of colitis that were tested (colon length, colonic myeloperoxidase activity, and

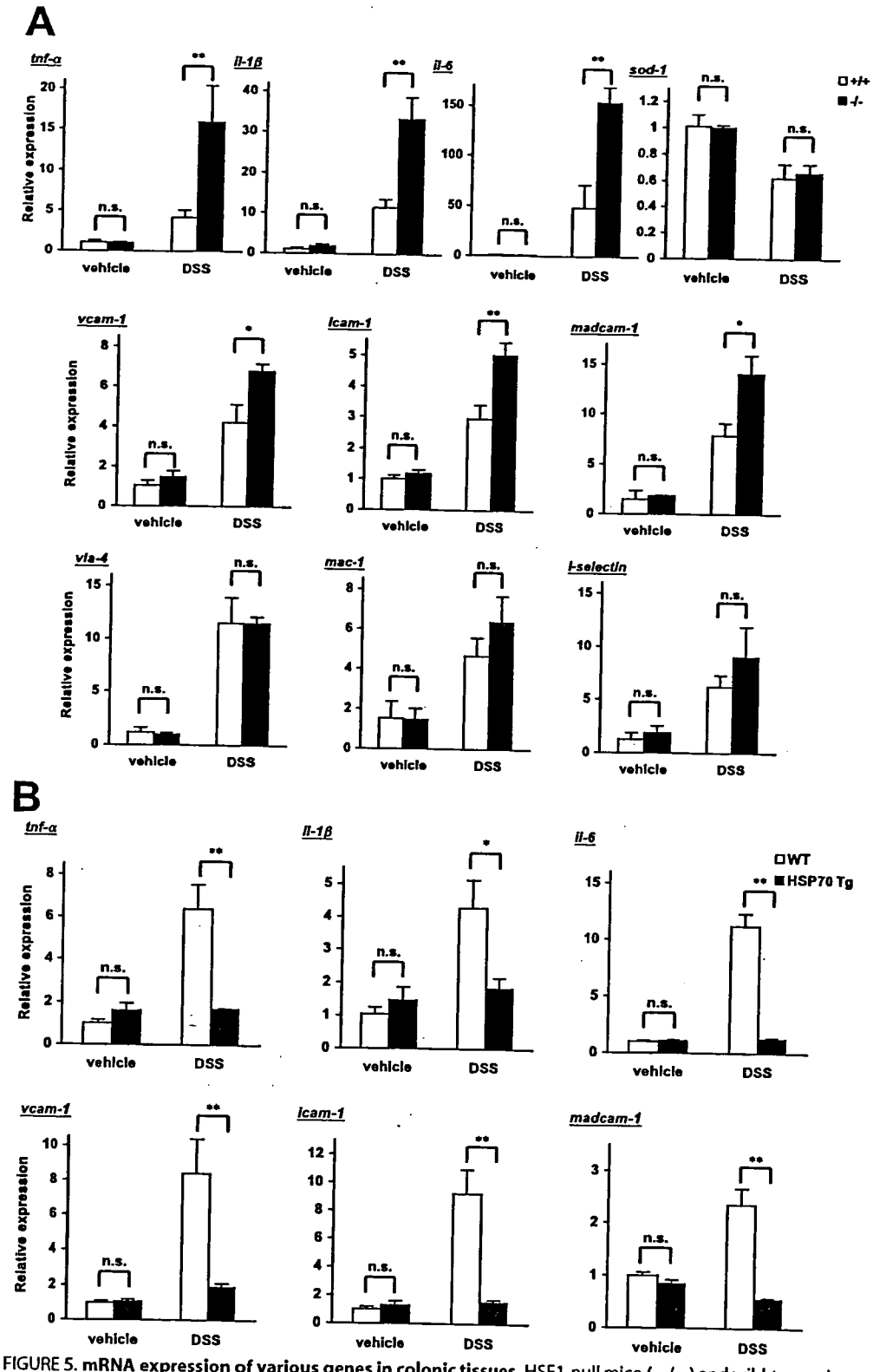

FIGURE 5. **mRNA expression of various genes in colonic tissues.** HSF1-null mice (−/−) and wild-type mice (+/+; ICR) (*A*) or transgenic mice expressing HSP70 (*HSP70 Tg*) and wild-type mice (*WT*; C57/BL6) (*B*) were treated with or without 3% DSS for 7 days. The relative mRNA expression of each gene in colonic tissues was monitored and is expressed as described in the legend of Fig. 2. Values are the mean ± S.E. (n = 3–6). *, $p < 0.05$; **, $p < 0.01$; *n.s.*, not significant.

colonic TBARS) showed that transgenic mice expressing HSP70 were more resistant than wild-type mice to DSS-induced colitis (Fig. 4, *C–E*). By immunohistochemical analysis, we confirmed that HSP70 expression was much higher in the colonic tissues of transgenic mice than in those of wild-type mice regardless of whether or not they were treated with DSS (Fig. 4*F*). The results in Fig. 4 suggest that HSP70 expression somehow suppresses DSS-induced colitis.

Involvement of Cytokines in Alteration of DSS-induced Colitis in HSF1-null Mice and Transgenic Mice Expressing HSP70—To understand the mechanism governing the increased susceptibility of HSF1-null mice to DSS-induced colitis, we compared the mRNA expression of various inflammation-related proteins in the colonic tissues. As shown in Fig. 5*A*, the mRNA expression of TNF-α, IL-1β, and IL-6 was much higher in DSS-treated HSF1-null mice than in wild-type mice. On the other hand, the mRNA expression of superoxide dismutase-1 was indistinguishable between HSF1-null and wild-type mice even after DSS administration (Fig. 5*A*). These results are consistent with the idea that the higher levels of mRNA expression of these pro-inflammatory cytokines in the colonic mucosa of HSF1-null mice are responsible for their increased susceptibility to DSS-induced colitis.

The mRNA expression of these pro-inflammatory cytokines was also compared in transgenic mice expressing HSP70 and wild-type mice. As shown in Fig. 5*B*, the mRNA expression of TNF-α, IL-1β, and IL-6 in colonic tissues was significantly lower in DSS-administered transgenic mice expressing HSP70 than in wild-type mice. These results are consistent with the idea that the lower mRNA expression of these pro-inflammatory cytokines in DSS-treated transgenic mice expressing HSP70 is responsible for their DSS-induced colitis resistance phenotype.

The results in Fig. 5 suggest that HSF1 and HSP70 negatively regulate the expression of the selected pro-inflammatory cytokines under inflammatory conditions. To test this idea *in vitro*, we compared the LPS-stimulated production of the pro-inflammatory cytokines

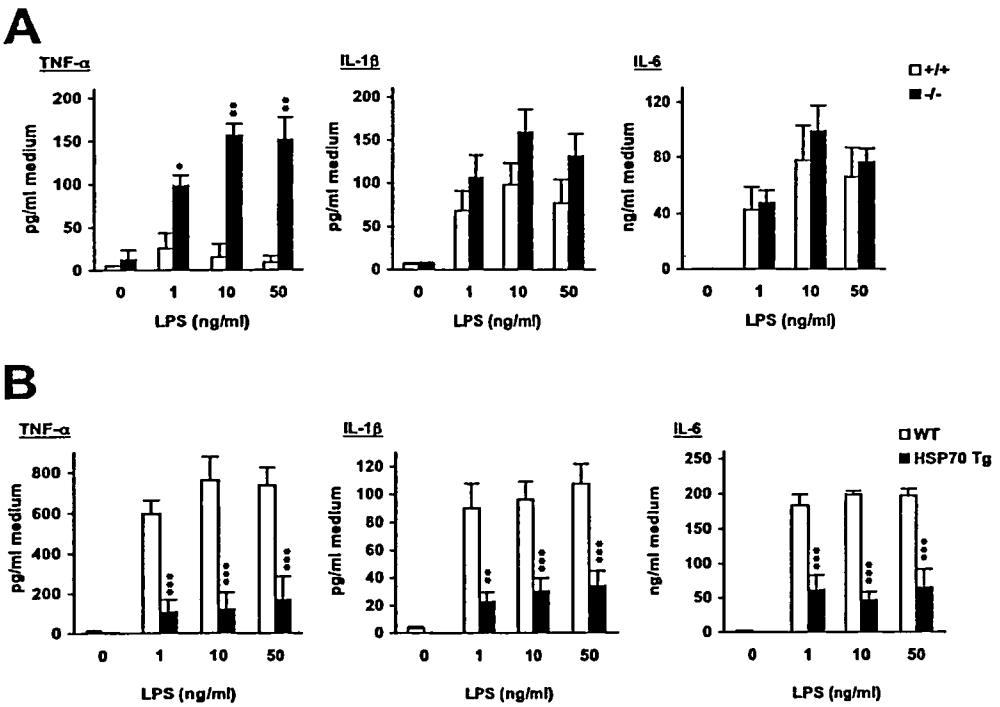

FIGURE 6. **LPS-stimulated production of pro-inflammatory cytokines in peritoneal macrophages.** Peritoneal macrophages were prepared from HSF1-null mice (−/−) and wild-type mice (+/+; ICR) (*A*) or transgenic mice expressing HSP70 (*HSP70 Tg*) and wild-type mice (*WT*; C57/BL6) (*B*) and incubated with the indicated concentrations of LPS for 24 h. The amount of each cytokine in the medium was determined by enzyme-linked immunosorbent assay. Values are the mean ± S.E. (n = 3–4). *, $p < 0.05$; **, $p < 0.01$; ***, $p < 0.001$.

(TNF-α, IL-1β, and IL-6) in peritoneal macrophages prepared from transgenic mice and their wild-type counterparts. As shown in Fig. 6*A*, LPS stimulated the production of all of these pro-inflammatory cytokines. The level of TNF-α was much higher in the medium of HSF1-null macrophages than in that of wild-type macrophages after LPS treatment; however, there was no significant difference in the levels of IL-1β and IL-6 between the two groups (Fig. 6*A*). These results suggest that HSF1 is involved in the production of TNF-α (but not IL-1β and IL-6) under inflammatory conditions.

In contrast, the levels of not only TNF-α but also of IL-1β and IL-6 were much lower in the medium of LPS-treated macrophages prepared from transgenic mice expressing HSP70 compared with wild-type mice. These results suggest that the expression of HSP70 may suppress the production of these pro-inflammatory cytokines under inflammatory conditions.

Involvement of CAMs in Altering the Susceptibility of HSF1-null Mice and Transgenic Mice Expressing HSP70 to DSS-induced Colitis—CAMs can be divided into two groups: those expressed mainly on vascular endothelial cells (such as VCAM-1, ICAM-1, and MAdCAM-1) and those expressed mainly on leukocytes (such as VLA-4, Mac-1, and L-selectin) (10). As shown in Fig. 5*A*, the mRNA expression of *vcam-1*, *icam-1*, and *madcam-1* in colonic tissues was higher in DSS-administered HSF1-null mice than in wild-type mice. In contrast, differences in the mRNA expression of *vla-4*, *mac-1*, and L-selectin in colonic tissues were not statistically significant between HSF1-null mice and their wild-type counterparts (Fig. 5*A*).

We also compared the mRNA expression of *vcam-1*, *icam-1* and *madcam-1* in the colonic tissues of transgenic mice expressing HSP70 and their wild-type counterparts. The mRNA expression of these CAMs was much lower in DSS-administered transgenic mice than in wild-type mice (Fig. 5*B*).

The results in Fig. 5 suggest that the expression of CAMs is negatively regulated by HSF1 and HSP70 under inflammatory conditions. To test this idea *in vitro*, we examined the effect of siRNA specific for HSF1 or HSP70 on the LPS-induced mRNA expression of the CAMs in bEnd.3 cells. Transfection with siRNA specific for HSF1 clearly inhibited the mRNA expression of *hsf1* in both the presence and absence of LPS (Fig. 7*A*). Transfection with HSF1 siRNA up-regulated the mRNA expression of *vcam-1* and *icam-1* but down-regulated that of *madcam-1* in the presence of LPS (Fig. 7*A*). These results suggest that HSF1 negatively regulates the mRNA expression of *vcam-1* and *icam-1* (but not *madcam-1*) under inflammatory conditions.

Transfection of the cells with siRNA specific for HSP70 inhibited the mRNA expression of *hsp70* in both the presence and absence of LPS. However, it did not significantly up-regulate the mRNA expression of the CAMs (but instead down-regulated the mRNA expression of *vcam-1*) in the presence of LPS, suggesting that, at least *in vitro*, HSP70 does not negatively regulate the mRNA expression of these CAMs under inflammatory conditions.

Involvement of ROS-induced Cell Death in Altering DSS-induced Colitis in HSF1-null Mice and Transgenic Mice Expressing HSP70—We compared the level of cell death in the colonic mucosa of DSS-administered HSF1-null mice or transgenic mice expressing HSP70 and the respective wild-type mice using the TUNEL assay. More TUNEL-positive cells (cell death) were observed in the colonic mucosa of DSS-administered HSF1-null mice than in that of wild-type mice (Fig. 8*A*). On the other hand, fewer TUNEL-positive cells were observed in the colonic mucosa of DSS-administered transgenic mice expressing HSP70 than in that of wild-type mice (Fig. 8*B*). The results suggest that ROS-induced cell death associated with DSS-induced colitis is stimulated or suppressed in HSF1-null mice or transgenic mice expressing HSP70, respectively.

To test the role of HSF1 and HSP70 in ROS-induced cell death *in vitro*, we examined the effect of siRNA specific for

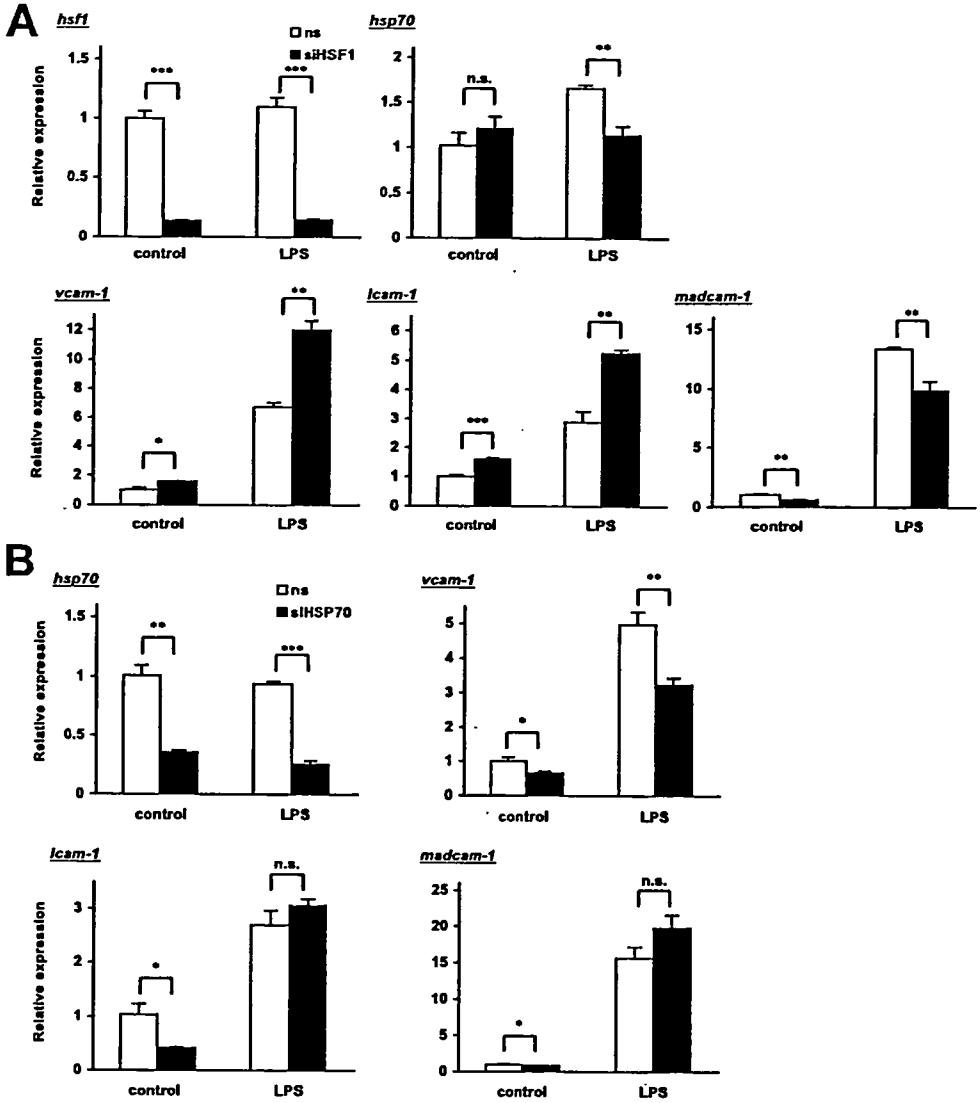

FIGURE 7. **Effect of siRNAs for HSF1 and HSP70 on the mRNA expression of various CAMs.** bEnd.3 cells were transfected with 1.2 μg of siRNA for HSF1 (*siHSF1*; *A*), siRNA for HSP70 (*siHSP70*; *B*), or non-silencing siRNA (*ns*; *A* and *B*). After 24 h, cells were incubated with or without 5 μg/ml LPS for 18 h. The relative mRNA expression of each gene was monitored and is expressed as described in the legend of Fig. 2. Values are the mean ± S.E. ($n = 3$). *, $p < 0.05$; **, $p < 0.01$; ***, $p < 0.001$; *n.s.*, not significant.

of cell death in colonic mucosa and the improved resistance to DSS-induced colitis observed in transgenic mice expressing HSP70.

DISCUSSION

A number of reports using HSF1-null mice and/or transgenic mice expressing HSP70 have shown that HSF1-dependent induction of HSP expression is protective against the development of various diseases, such as gastric ulcers, heart failure, pancreatitis, hypoxic/ischemic brain injury, and spinal and bulbar muscular atrophy (42–46). Because some HSPs have been reported to be overexpressed in the intestinal tissues of IBD patients (19, 20, 23) and in an animal model of IBD (21–23). HSF1 and HSPs are thought to be involved in the pathogenesis of IBD. However, as was described in the Introduction, some studies have suggested that these proteins inhibit and others have suggested that they promote the development of IBD. In this study, we have gathered evidence that HSF1 and HSPs have negative roles in the development of IBD (protective roles against IBD) by demonstrating the sensitive phenotype of HSF1-null mice and the resistant phenotype of transgenic mice expressing HSP70 (or HSF1) against DSS-induced colitis, an animal model for IBD. Proposed mechanisms for positive roles of HSF1 and HSP70 in the development of IBD (such as immunoactivation by extracellular HSPs) may be present; however, these effects may be masked by the protective roles of HSF1 and HSP70 against DSS-induced colitis (see below). This study provides the first genetic evidence for involvement of HSF1 and HSPs in IBD-related colitis. Furthermore, we have examined the molecular mechanisms governing the susceptibility of HSF1-null mice and transgenic mice expressing HSP70 to DSS-induced colitis, focusing on the expression of pro-inflammatory cytokines and CAMs and ROS-induced cell death both *in vivo* and *in vitro* (see below).

Pro-inflammatory cytokines (in particular, TNF-α) positively contribute to the progression of IBD and colitis in animal models of IBD (6, 7). DSS-induced mRNA expression of various pro-inflammatory cytokines (TNF-α, IL-1β, and

HSF1 or HSP70 on cell death induced by menadione, a superoxide anion (a representative ROS)-releasing drug, in a colon cancer cell line (HCT-15). Transfection of these cells with siRNA for HSF1 clearly inhibited the mRNA expression of *hsf1* in both the presence and absence of menadione (Fig. 9*A*). As shown in Fig. 9*B*, treatment of cells with menadione induced cell death in a dose-dependent manner. Transfection of cells with HSF1 siRNA did not clearly affect menadione-induced cell death. (A slight stimulation of cell death was observed with 50 μM menadione.) On the other hand, transfection of cells with siRNA for HSP70 inhibited the mRNA expression of *hsp70* in both the presence and absence of menadione (Fig. 9*C*) and clearly stimulated cell death induced by menadione, but did not affect cell viability in the absence of menadione (Fig. 9*D*). The results in Fig. 9 suggest that HSP70 protects colonic cells from ROS-induced cell death and that this effect may be involved in the lower level

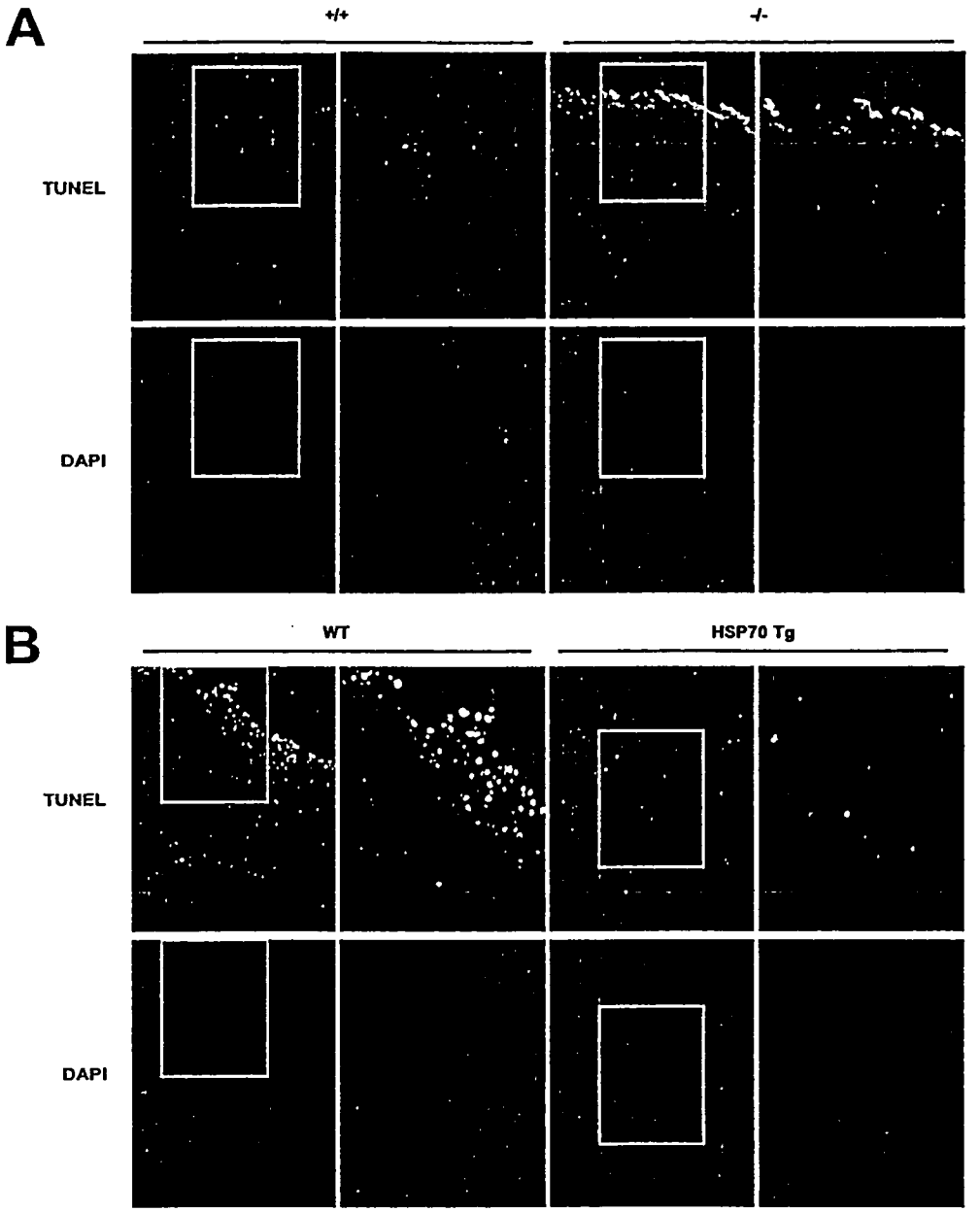

FIGURE 8. **Levels of cell death in colonic mucosa after DSS administration.** HSF1-null mice (−/−) and their wild-type counterparts (+/+; ICR) (*A*) or transgenic mice expressing HSP70 (*HSP70 Tg*) and their wild-type counterparts (*WT*; C57/BL6) (*B*) were administered 3% DSS for 7 days. Sections of colonic tissues were prepared and subjected to TUNEL assay and 4′,6-diamidino-2-phenylindole (*DAPI*) staining. The *right panel* in each grouping is a twice-magnified image of the *boxed area* in the *left panel*.

IL-6) in colonic tissues was stimulated or inhibited in HSF1-null mice or transgenic mice expressing HSP70, respectively. We consider that this stimulation or inhibition of cytokine mRNA expression is responsible for the DSS-induced colitis phenotypes exhibited by these mice. Because the observation that deficiency of HSF1 stimulates the production of TNF-α (but not IL-1β and IL-6) was reproduced *in vitro* (in the model of LPS-induced production of pro-inflammatory cytokines in peritoneal macrophages), HSF1 seems to be directly involved in the expression of TNF-α, but not IL-1β and IL-6. HSF1 suppresses the mRNA expression of TNF-α through binding to the heat shock element located in the promoter of TNF-α as described previously (25). Because TNF-α secondarily stimulates the production of many other pro-inflammatory cytokines, including IL-1β and IL-6 (9), the higher mRNA expression of IL-1β and IL-6 seen in HSF1-null mice relative to control mice could be mediated by TNF-α. On the other hand, the LPS-induced production of not only TNF-α but also IL-1β and IL-6 was inhibited in peritoneal macrophages prepared from transgenic mice expressing HSP70, suggesting that HSP70 suppresses the production of these pro-inflammatory cytokines under inflammatory conditions. We speculate that this suppression is mediated by HSP70-dependent inhibition of NF-κB, which plays an important role in the induction of inflammation. It is known that NF-κB positively regulates the expression of pro-inflammatory cytokines, including TNF-α, IL-1β, and IL-6. Furthermore, it is also known that up-regulation of HSP70 expression by heat shock inhibits the inflammatory stimuli-dependent activation of NF-κB through various mechanisms (47–52).

CAMs also positively contribute to the progression of IBD and colitis in animal models of IBD through recruitment of blood circulating leukocytes into inflamed intestinal tissues (10). DSS administration induced the mRNA expression of CAMs expressed mainly on vascular endothelial cells and leukocytes. However, HSF1 deficiency affected only the mRNA expression of CAMs on vascular endothelial cells, suggesting that these CAMs rather than those on leukocytes contribute to the greater sensitivity of HSF1-null mice to DSS-induced colitis relative to control wild-type mice. The DSS-induced mRNA expression of *icam-1*, *vcam-1*, and *madcam-1* was suppressed in transgenic mice expressing HSP70, and this may be involved in conferring resistance to DSS-induced colitis. *In vitro*, transfection with HSF1 siRNA stimulated the LPS-induced mRNA expression of *icam-1* and *vcam-1*, suggesting that HSF1 negatively regulates the mRNA expression of *icam-1* and *vcam-1*, which seems to be responsible for the higher levels of mRNA expression of these CAMs in HSF1-null mice